MODELING OF MASS TRANSFER AND REACTIONS WITH THE MOMENT METHOD

Zheng Liu

Aalto University

DOCTORAL DISSERTATIONS

MODELING OF MASS TRANSFER AND REACTIONS WITH THE MOMENT METHOD

Zheng Liu

Aalto University
School of Chemical Technology
Department of Biotechnology and Chemical Technology
Research Group of Chemical Engineering

Supervising professor
Prof. Dr. Ville Alopaeus

Preliminary examiners
Prof. Dr. Alírio E. Rodrigues, Universidade do Porto, Portugal
Prof. Dr. Tingyue Gu, Ohio University, USA

Opponent
Dr. Eric von Lieres, Forschungszentrum Jülich GmbH, Germany

NORDIC ECOLABEL

441   697
Printed matter

Abstract

In chemical engineering field, mass transfer and reaction process models are needed in many stages of process research and design. These models usually consist of systems of partial differential equations. The focus of this work is to study the moment method as a numerical tool to solve different mass transfer and reaction models, which can be utilized to simulate a number of chemical engineering processes e.g. chromatography, adsorption, extraction etc.

The implementation procedures, the features of the moment method are introduced with different application cases in this work. The moment transformation procedure, as the key step of the moment method is discussed in great detail when the moment method is applied to solve the chromatographic model. The important features of the moment method revealed in this work include: 1) Similar with other higher order methods, the moment method reaches desired accuracy with decreased number of variables and reduced computational load; 2) The moment method predicts the chromatographic effluent curve moments with good accuracy, because the moment method is to minimize the errors in the column profile moments; 3) Based on the moment method, the spatial PDE solution inherently conserves mass if 0th order moment is included into the set of equations.

Different mass transfer and reaction processes are modeled in this work. From modeling point of view, these models are highly similar to each other except some minor details e.g. boundary conditions. This characteristic naturally is beneficial for the implementation of modeling tasks.

Preface

I did my PhD study and research for this dissertation in the Chemical Engineering Research Group at the Department of Biotechnology and Chemical Technology, School of Science and Technology at Aalto University between July 2010 and Aug 2014. During this period I received a lot of supports, contributions for my work, without which it is not possible to finalize my PhD study. Hence I would take this opportunity to express my appreciation to all the people and organizations concerned.

Needless to say, my most special thankfulness goes to my supervising Professor Ville Alopaeus. His guidance and instructions are the necessities for me during my study. More impressively, his hard-working spirit has been continuously encouraging me, especially at the moments when my research went into darkness. Without his contributions, this work would not be possible, even from the very beginning of my study.

I would also express my appreciation to my other co-authors, Dr. Jonas Roininen, Dr. Iiro Pulkkinen, Dr. Pia Saari, Prof. Tuomo Sainio, Dr. Susanna Kuitunen, Ville Suntio and Waqar Ahmad for their contributions to my publications and to this thesis. Also I would thank Lasse Westerlund and Sirpa Aaltonen for their supports in administrative issues.

At last, I would show my deep thankfulness to my wife, my daughters and my parents for their emotional support and encouragement during my study.

Otaniemi, Espoo, July 23, 2014

Zheng Liu

List of Publications

In this thesis, 4 publications are contained as listed in the followings.

[1] Liu, Z., Roininen, J., Pulkkinen, I., Sainio, T., & Alopaeus, V., Moment Based Weighted Residual Method–New Numerical Tool for a Nonlinear Multicomponent Chromatographic General Rate Model, *Comput. Chem. Eng* (2013), 53, 153-163.

[2] Liu, Z., Roininen, J., Pulkkinen, I., Saari, P., Sainio, T., & Alopaeus, V., A New Moment Analysis Method to Estimate the Characteristic Parameters in Chromatographic General Rate Model, *Comput. Chem. Eng* (2013), 55, 50-60.

[3] Liu, Z., Suntio, V., Kuitunen, S., Roininen, J., & Alopaeus, V., Modeling of mass transfer and reactions in anisotropic biomass particles with reduced computational load, *Ind. Eng. Chem. Res* (2014), 55, 4096-4103.

[4] Liu, Z., Ahmad, W., Kuitunen, S., & Alopaeus, V., Modeling of mass transfer and degradation of hemicelluloses in flow-through hot water extraction, *Nordic Pulp & Paper Research Journal* (2014), 29, 568-583.

Author's Contributions to the Publications

[1] The author developed, solved and verified the models, analyzed the results with the co-authors, and wrote the paper.

[2] The author fitted the model parameters against the data, analyzed the results with the co-authors, and wrote the paper.

[3] The author developed the models, performed the calculations, analyzed the results with the co-authors, and wrote the paper.

[4] The author developed the models, fitted the model parameters against the data, verified the models, analyzed the results with the co-authors, and wrote the paper.

1. Introduction

Theory based analysis, experiments and mathematical modeling are the three methodologies to push forward the development in chemical engineering, and most likely in other scientific fields. In present, the applications of mathematical modeling are significantly critical in chemical engineering research, equipment design and process optimization. Mathematical modeling is, by name, a mathematical description or abstraction of the realistic world. However this description in all conditions deviates more or less from the reality and has always been a compromise between the feasibility and accuracy. In the past decades, the computational power has developed rapidly. For this reason, more complicated models can be utilized to simulate the reality with limited errors, which provides great benefits for the chemical engineers.

For the implementation of modeling and simulation, the use of efficient numerical algorithms is usually needed to solve the mathematical equations. Two classes of methods are commonly applied as the numerical algorithms in the modeling tasks of chemical engineering. One class of methods is based on the discretization of original governing model equations. The other class is the weighted residual methods, containing a number of different sub-methods. The main subject of this thesis is the study of novel applications of the moment based weighted residual method (or simplified as "the moment method"), as one sub-method in the class of weighted residual methods. In addition, to demonstrate different applications of the classical mass transfer and reaction models is another important topic discussed in this thesis.

Two publications (Alopaeus et al., 2008; Roininen et al., 2010) are considered as the starting point of this thesis. Alopaeus et al., presented the procedure to solve a dynamic model for plug flow reactor with the moment method. Roininen et al., applied the moment method to solve the dynamic model with axial dispersion term. In this thesis, the applications of the moment method are developed further as presented in the application section and in the attached publications.

Four publications are included in this thesis, namely [1]-[4]. Publication [1] discusses the implementation details of the moment method to solve the chromatographic general rate model which is characterized as coupled partial differential equations. Publication [2] provides a novel method for parameter fittings according to the moments of the chromatographic effluent curves. Publication [3] presents the procedures to reduce the computational load when solving the concentration profiles in anisotropic biomass particles by: 1) to simplify the three dimensional model into one dimensional; 2) to solve the model with high order moment method, instead of the commonly used low order finite difference method. In Publication [4], a model is developed to describe the mass transfer and degradation of hemicellulose in flow-through hot water extraction processes. The moment method is applied as an efficient numerical tool to solve the model.

2. Mass transfer models in chemical engineering

Chemical engineering a hundred years ago was mainly considered as an industry, consisting of a number of independent product related techniques. During that period, the research and study were in principle based on these techniques, such as fertilizer manufacture process, sugar and salt production techniques etc. From 1920s to 1950s with the accumulated experience and knowledge, it was recognized that different techniques and processes in chemical engineering can be divided into a number of individual unit operations. The typical unit operations include, e.g. evaporation, filtration, distillation, extraction, heating, cooling, absorption, crystallization etc. Since 1950s with the study proceeded further in unit operations, it was found that similarities in different unit operations existed. For example heating and cooling are related to heat transfer; absorption and extraction can be characterized as mass transfer process; evaporation and distillation are the combination of heat transfer and mass transfer etc. (Chen & Zhang, 2001)

R.B.Bird, S.E.Stewart, E.N.Lightfoot published the book named "Transport Phenomena" (Bird et al., 1960), which was considered as a milestone in the development of chemical engineering field. In this book, the basic theories of momentum transfer, heat transfer and mass transfer were systematically introduced for the first time. Since then, the transfer theories became one of the most important research topics in chemical engineering field. However at 1960s, the computational tools available to solve the transfer problems were still limited. In recent decades with the rapid development in computational power and numerical methods, chemical engineers and researchers obtained a lot more opportunities to solve the chemical engineering problems based on the transfer theories.

Since mass transfer is the main focus of this thesis, the general formulations of the mass transfer models are discussed in detail in this section. Several classical models to describe diffusion and convection are introduced as well.

2.1 Mass transfer models – general formulations

In this part, the general formulations of the mass transfer models and brief derivation procedures (Wang, 2004; Chen & Zhang 2001) are presented and discussed. In the case where mass transfer proceeds with unsteady state conditions in a multi-component system with the fluid phase flowing in all directions, partial differential equations are needed to describe the mass transfer process. Here assumption is made that the mass transfer of solute A proceeds in solution B. The derivations of model equations can be formulated according to molar mass concentration or mass concentration. The former is used to present the model derivations in this section, since the models in the publications included in this thesis are mainly with molar mass concentration. One micro element of rectangular shape in the fluid phase is employed in the derivation as shown in Figure 2.1.
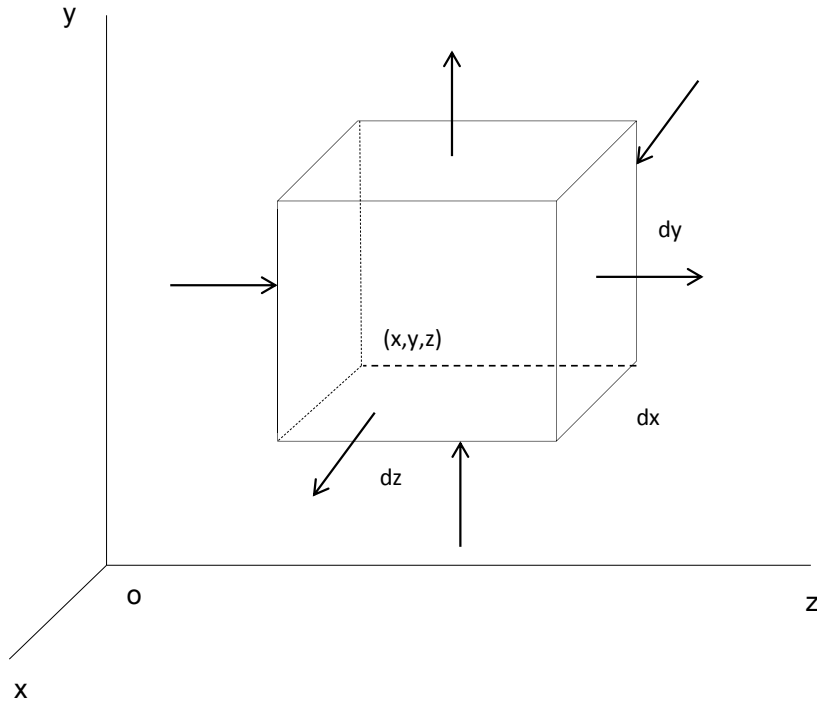
Figure 2.1 Layout of differential control volume

If solute A (mol/L^3) is the study objective, according to the mass conservation law we have:

"mass transfer input rate of A into the element" + "mass generation rate of A in the element by reactions" = "mass transfer output rate of A out of the element" + "accumulation rate of A in the element"

The statement can be written in a simplified notion as:

Output – Input + Accumulation – Generation = 0   (2.1)

This is the expression of mass conservation law. In the followings, each term in the expression is analyzed in order to derive the general formulations of the mass transfer model.

2.1.1 Mass transfer rate

In point (x, y, z), it is assumed that the fluid flow rate is u (molar average velocity). The flow rates in each dimension of the Cartesian coordinates is u_x, u_y, u_z. The fluxes due to the flow of fluid or convection in all the three directions are $C_A u_x, C_A u_y, C_A u_z$. The molar

flux relative to the molar average velocity due to diffusion in all the three directions are j_{Ax}, j_{Ay}, j_{Az}.

The input rate of solute A along the x direction from the left side area is:

$$Input_x = (C_A u_x + j_{A,x})dydz \tag{2.2}$$

The output rate of solute A along the x direction from the right side area is:

$$Output_x = \left[(C_A u_x + j_{A,x}) + \frac{\partial(C_A u_x + j_{A,x})}{\partial x} dx \right] dydz \tag{2.3}$$

The difference of output and input rate is:

$$(Output - Input)_x = \left[\frac{\partial(C_A u_x)}{\partial x} + \frac{\partial j_{A,x}}{\partial x} \right] dxdydz \tag{2.4}$$

Similarly the differences of output and input rate along y, z directions are:

$$(Output - Input)_y = \left[\frac{\partial(C_A u_y)}{\partial y} + \frac{\partial j_{A,y}}{\partial y} \right] dxdydz \tag{2.5}$$

$$(Output - Input)_z = \left[\frac{\partial(C_A u_z)}{\partial z} + \frac{\partial j_{A,z}}{\partial z} \right] dxdydz \tag{2.6}$$

The total difference of output and input rate in all three directions is:

$$Output - Input = \left[\frac{\partial(C_A u_x)}{\partial x} + \frac{\partial(C_A u_y)}{\partial y} + \frac{\partial(C_A u_z)}{\partial z} + \frac{\partial j_{A,x}}{\partial x} + \frac{\partial j_{A,y}}{\partial y} + \frac{\partial j_{A,z}}{\partial z} \right] dxdydz \tag{2.7}$$

2.1.2 Accumulation rate

The concentration of solute A is C_A, and $C_A = f(x,y,z,t)$. The number of moles of A at an instant moment in the micro element is:

$$N_A = C_A dxdydz \tag{2.8}$$

The accumulation rate of A is:

$$\frac{\partial N_A}{\partial t} = \frac{\partial C_A}{\partial t} dxdydz \tag{2.9}$$

4

2.1.3 Generation rate

If reaction exists in the system, the reaction rate in the micro element is r_A. When A is product, r_A is positive; when A is reactant, r_A is negative. The generation rate of A is:

$$Generation \ \ Rate = r_A dxdydz \tag{2.10}$$

2.1.4 Mass transfer differential models

When inserting Eq.(2.7), (2.9) and (2.10) into Eq.(2.1), the equation becomes:

$$\frac{\partial(C_A u_x)}{\partial x} + \frac{\partial(C_A u_y)}{\partial y} + \frac{\partial(C_A u_z)}{\partial z} + \frac{\partial j_{A,x}}{\partial x} + \frac{\partial j_{A,y}}{\partial y} + \frac{\partial j_{A,z}}{\partial z} + \frac{\partial C_A}{\partial t} - r_A = 0 \tag{2.11}$$

Eq.(2.11) is transformed as:

$$C_A\left(\frac{\partial u_x}{\partial x} + \frac{\partial u_y}{\partial y} + \frac{\partial u_z}{\partial z}\right) + \frac{DC_A}{Dt} + \frac{\partial j_{A,x}}{\partial x} + \frac{\partial j_{A,y}}{\partial y} + \frac{\partial j_{A,z}}{\partial z} - r_A = 0 \tag{2.12}$$

Where the total derivative of concentration is defined as:

$$\frac{DC_A}{Dt} = \frac{\partial C_A}{\partial t} + u_x\frac{\partial C_A}{\partial x} + u_y\frac{\partial C_A}{\partial y} + u_z\frac{\partial C_A}{\partial z} \tag{2.13}$$

According to Fick's law:

$$j_{Ax} = -D_{AB}\frac{\partial C_A}{\partial x} \tag{2.14a}$$

$$j_{Ay} = -D_{AB}\frac{\partial C_A}{\partial y} \tag{2.14b}$$

$$j_{Az} = -D_{AB}\frac{\partial C_A}{\partial z} \tag{2.14c}$$

Eq. (2.12) is rearranged as:

$$C_A\left(\frac{\partial u_x}{\partial x} + \frac{\partial u_y}{\partial y} + \frac{\partial u_z}{\partial z}\right) + \frac{DC_A}{Dt} = D_{AB}\left(\frac{\partial^2 C_A}{\partial x^2} + \frac{\partial^2 C_A}{\partial y^2} + \frac{\partial^2 C_A}{\partial z^2}\right) + r_A \tag{2.15}$$

The vector notation of Eq.(2.15) is:

$$C_A(\nabla \bullet u) + \frac{DC_A}{Dt} = D_{AB}\nabla^2 C_A + r_A \tag{2.16}$$

Eq. (2.16) is the general mass transfer differential model.

Similar as Eq.(2.15), the model equation in spherical coordinate is:

$$\frac{\partial C_A}{\partial t} + u_r \frac{\partial C_A}{\partial r} + \frac{u_\omega}{r}\frac{\partial C_A}{\partial \omega} + \frac{u_\phi}{r\sin\omega}\frac{\partial C_A}{\partial \phi} = D_{AB}\left[\frac{1}{r^2}\frac{\partial}{\partial r}\left(r^2\frac{\partial C_A}{\partial r}\right) + \frac{1}{r^2\sin\omega}\frac{\partial}{\partial\omega}\left(\sin\omega\frac{\partial C_A}{\partial\omega}\right) + \frac{1}{r^2\sin\omega^2}\frac{\partial^2 C_A}{\partial\phi^2}\right] + r_A$$

$$\tag{2.17}$$

t is time, r is radius coordinate, ϕ is angle of position, ω is colatitude, u_r, u_ϕ, u_ω are the components of the mass average speed in spherical coordinates (r, ϕ, ω).

The one dimensional mass transfer models applied in the publications of this thesis were modified from the general mass transfer differential models as in Eq.(2.15) and (2.17).

2.2 Estimation of diffusion coefficients

In the mass transfer models, diffusion coefficients need to be predicted with accuracy. Three methods are introduced in the following for estimating the diffusion coefficients.

2.2.1 Stokes-Einstein theory

The Stokes-Einstein equation was firstly published in (Einstein, 1905) on the theory of Brownian motion. The equation is mainly used for the diffusion of spherical particles or molecular in diluted solution with certain dynamic viscosity at absolute temperature T.

$$D_{AB} = \frac{kT}{6\pi\mu_B r_A}$$

r_A: Molecular radius of solute A, m
μ_B: Dynamic viscosity of solvent B, in cP
k: Boltzmann constant
T: Temperature in Kelvin

The value of this theory depicts the relationship between the diffusion coefficient D_{AB} and the dynamic viscosity μ_B, which provides the theoretical foundation for other complementary empirical formulations.

2.2.2 Wilke-Chang semi-empirical formulation

Wilke-Chang formulation (Wilke & Chang, 1955) is as:

$$D_{AB} = 7.4 \times 10^{-12} (\Phi M_B)^{1/2} \frac{kT}{\mu_B V_{bA}^{0.6}}$$

M_B: Molar mass of solvent B

Φ: Associative factor of solvent B (e.g. $\Phi_{water} = 2.6$, $\Phi_{ethanol} = 1.5$, $\Phi = 1.0$ for non-associative solvent)

V_{bA}: Molecular volume of solute A at the boiling point under standard atmosphere pressure

For non-electrolyte diluted solution and small molecular, the deviation between the predicted and measured diffusion coefficients is within approximately 13.0% (Chen & Zhang, 2001).

2.2.3 Scheibel semi-empirical formulation

Another semi-empirical formulation to estimate the diffusion coefficient is (Liong et al., 1991):

$$D_{AB} = 8.2 \times 10^{-12} \left[1 + \left(\frac{3V_{bB}}{V_{bA}} \right)^{2/3} \right] \frac{T}{\mu_B V_{bA}^{1/3}}$$

V_{bA}: Molecular volume of solute A at the boiling point under standard atmosphere pressure

V_{bB}: Molecular volume of solvent B at the boiling point under standard atmosphere pressure

This formulation above is applicable also for diluted solution. In some cases, it appears to be more exact than the preceding one; but for $v_A/v_B \leq$ (1 - 2), the deviation from experiment becomes important. The Scheibel method typically yields estimates with errors of < 20% for diffusion coefficients in organic solvents (Thibodeaux & Mackay, 2011).

2.3 Mass transfer models across phase boundaries

The estimation of mass flux across the phase boundaries is critical in the applications of mass transfer models. Assumptions are usually made to construct descriptive mathematic models for the mass flux. Three representative models, Two film model, Higbie model and Danckwerts model are discussed in this section.

1) Two film model

Two film theory, also referred as steady film theory was proposed in (Lewis & Whitman, 1924). This was the first model describing the convection mass transfer and has been applied widely till now as the standard model for estimating the mass and heat transfer fluxes across phase boundaries.

The most basic assumption is that two very thin films locate on both sides of the interface of two phases. Mass transfer resistance exists only in the two adjacent thin films. The turbulent flow pattern in the bulk phases disappears when it approaches to the interface. The molecular diffusion through the two films becomes the dominant manner for mass transfer. The interphase between the films is in thermodynamic equilibrium. No accumulation of mass or energy is in the films. Figure 2.2 shows a schematic representation of the two film model.
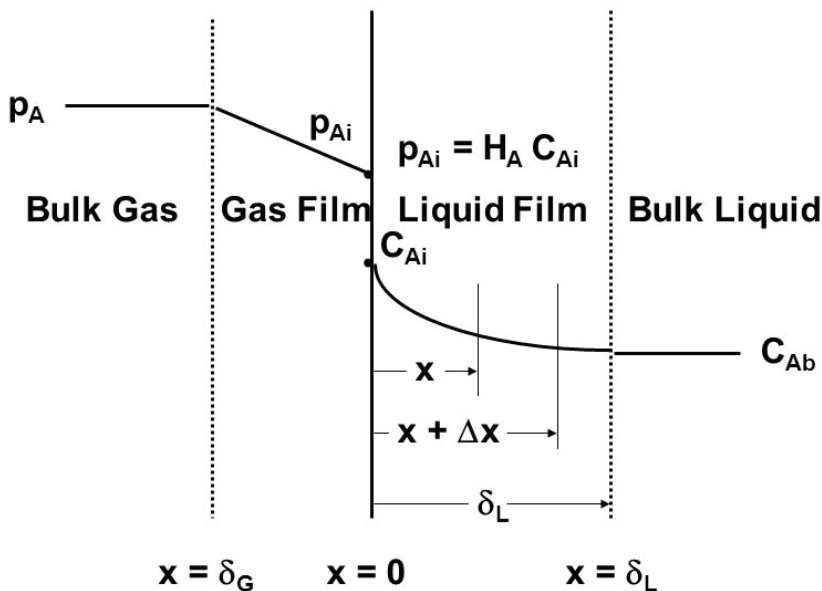

Figure 2.2 Schematic layout of the two film model (Lewis & Whitman, 1924)

Two film model provides the theoretical foundation for the theory of mass transfer. However, the simplified mass transfer mechanism results in sometimes unexpected errors when describing fast mass transfer process in industrial applications, e.g. highly efficient packing tower (Taylor & Krishna, 1993).

2) Higbie penetration model

The Higbie penetration model was proposed by Higbie (Higbie, 1935) to illustrate the transfer mechanism of solute from the liquid phase through the interface. The model states

that diffusion is in unsteady state and the molecules of the solute are in constant random motion. The clusters of these molecules arrive at the interface, remaining there for a fixed period of time. Some of the molecules penetrate into the liquid phase. Some of them mix back into the bulk of the gas phase (Hines & Maddox, 1985). Figure 2.3 shows the schematic layout of the Higbie penetration model.
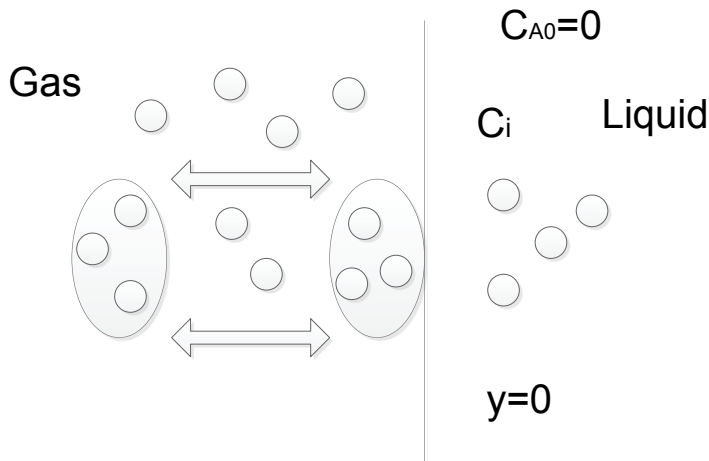

Figure 2.3 Schematic layout of the Higbie penetration model

The formulation to calculate the convection mass transfer coefficient is derived based on the Fick's second law. The derivation procedure is found in (Higbie, 1935). The formulation is:

$$k_{cm} = 2\sqrt{\frac{D_{AB}}{\pi\theta_c}}$$

k_{cm} : the convection mass transfer coefficient

D_{AB} : diffusion coefficient of solute A in solvant B

θ_c : remaining time of the solute at the interface

Danckwerts modified the Higbie penetration theory. This model is similar to Higbie model, except that molecules at the interface remain for different random periods of time or for different age (Danckwerts, 1951).

3. Numerical methods for mass transfer models

3.1 Introduction of numerical methods

Most mass transfer models, as well as other chemical engineering models include complicated partial differential equations with multiple dimensions. Analytical solutions are available only in very limited cases for these models. Therefore a number of numerical methods have been developed in order to solve the models (Rice and Do, 1995).

In this section, the most traditional computational techniques based on discretization are firstly introduced. The underlining idea of these techniques, as shown in Figure 3.1, is to discretize the governing partial differential equations into a system of algebraic equations, which are solved consequently. The most commonly used techniques include the finite difference, finite element, finite volume and spectral methods (Fletcher, 1991). As the two most important and most frequently used methods, the differences and similarities of finite difference and finite volume methods are discussed. In addition, the features of higher order and low order numerical methods are presented briefly by a number of representative examples.
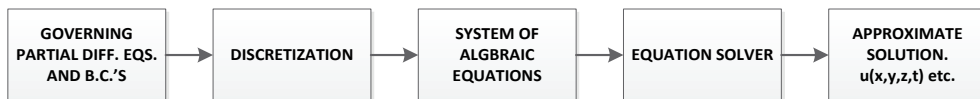

Figure 3.1. Overview of the computational solution procedure (Fletcher, 1991)

Weighted residual methods, different in nature from the discretization methods, are presented also in this section. The fundamentals of weighted residual methods are that it assumes the existence of an approximate solution. The methods can be also described by Figure 3.1, if the second box "discretization" is replaced by "parameterization with trial functions". Various methods belong to this category are discussed such as subdomain method, least squares method, collocation method, Galerkin method, moment method.

3.2 Finite Difference Method

To discretize the governing partial differential equations to a system of algebraic equations or ordinary differential equations, finite difference method is the most widely applied technique with probably as long history as calculus itself. Detailed discussions of the finite difference methods can be found in (Fletcher, 1991; Finlayson, 1980; Wang, 2004; Ferziger & Peric, 2002). Equation (3.1) is the definition of a derivative, which reflects also the foundation of finite difference method.

$$\frac{\partial \Psi}{\partial x} = \lim_{\Delta x \to 0} \frac{\Psi(x + \Delta x) - \Psi(x)}{\Delta x} \tag{3.1}$$

One example of a single Taylor series expansions with three expansion terms as in Eq (3.2) (Fletcher, 1991),

$$\Psi_{i+1} = \Psi_i + \Delta x \left[\frac{\partial \Psi}{\partial x} \right]_i + \frac{\Delta x^2}{2} \left[\frac{\partial^2 \Psi}{\partial x^2} \right]_i + O(\Delta x^3) \tag{3.2}$$

where $O(\Delta x^3)$ represents the error of the approximation. We may write two discretization based approximation method of the first spatial derivative:

Forward difference:

$$\left. \frac{\partial \Psi}{\partial x} \right|_i \approx \frac{\Psi_{i+1} - \Psi_i}{\Delta x} \tag{3.3}$$

Backward difference:

$$\left. \frac{\partial \Psi}{\partial x} \right|_i \approx \frac{\Psi_i - \Psi_{i-1}}{\Delta x} \tag{3.4}$$

From a more general methodical technique for constructing difference approximations in Eq. (3.5) (Fletcher, 1991),

$$\left[\frac{\partial \Psi}{\partial x} \right]_i = a\Psi_{i-1} + b\Psi_i + c\Psi_{i+1} + O(\Delta x^m) \tag{3.5}$$

where a, b and c are to be determined and the term $O(\Delta x^m)$ will indicate the accuracy of the resulting approximation. m is three and related to the number of terms on the right hand side of Eq.(3.5). We may write the central difference method to approximate the first spatial derivative and the approximation of the second spatial derivative as:

Central difference:

$$\left. \frac{\partial \Psi}{\partial x} \right|_i \approx \frac{\Psi_{i+1} - \Psi_{i-1}}{2\Delta x} \tag{3.6}$$

The second spatial derivative is:

$$\left. \frac{d^2 \Psi}{dx^2} \right|_i \approx \frac{\Psi_{i+1} - 2\Psi_i + \Psi_{i-1}}{\Delta x^2} \tag{3.7}$$

The discretization of time derivative $\dfrac{\partial \Psi}{\partial t}$ is similar as for the spatial discretization. The time discretization based on the backward difference is shown in Eq.(3.8). n indicates the time level with known information Ψ^n. However, information from time level $n+1$ and greater is not available because time proceeds only in positive direction. This discretization is called as backward Euler method or implicit Euler method, which is unconditionally stable (Atkinson, 1989).

$$\frac{\partial \Psi}{\partial x} \approx \frac{\Psi^{n+1} - \Psi^n}{\Delta t} \tag{3.8}$$

The basis for the finite difference method is the construction of a discrete grid, the replacement of the continuous derivatives in the partial differential equations with equivalent finite difference expressions and the rearrangement of the resulting algebraic equation into an algorithm (Fletcher, 1991). A flowchart describing the implementation steps of the finite difference method is:
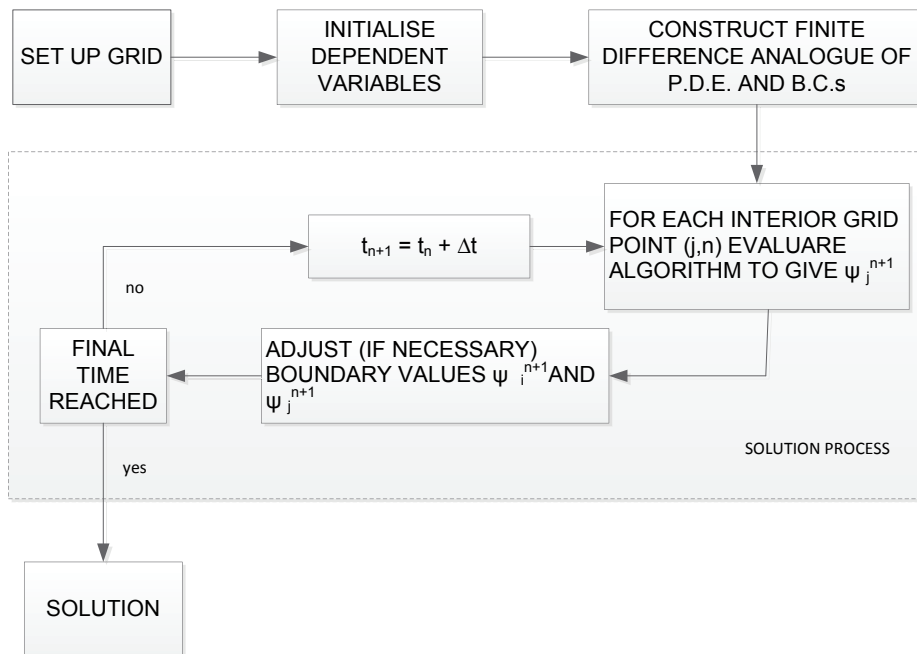

Figure 3.2 Schematic of the finite difference solution process (Fletcher, 1991)

In practical implementation of the finite difference method, very often only the spatial term in the partial differential equation is discretized. By doing so, the governing partial differential equations are reduced to a system of ordinary differential equations at the nodal points. This system can be considered as a semi-discrete form, or known as the method of lines. With the development of a number of techniques that are used for the

systems of ordinary differential equations, the method of lines becomes very attractive because the techniques can be applied conveniently to solve the semi-discrete form of the partial differential equations (Schiesser & Griffiths, 2009).

3.3 Finite Volume Methods

Finite volume methods, or named as control volume methods have recently attracted great attention and been developed to a high level mainly for computational fluid dynamics applications. The features of fluid dynamics problems include complex geometries with two and three dimensions, which can be adopted and solved conveniently by the finite volume methods.

The basic idea of the finite volume method is to divide the computational domain into a number of control volumes; volume integral is applied to the governing equations in order to obtain a group of discretized functions. This basic idea differs the finite volume method from other discretization methods. After the discretization process on the continuous computational domain is completed, four geometric conditions can be obtained as:

1) Node point: is the geometric location of the unknown variable, representing the according control volume.
2) Control volume: is the integration domain for the governing equations.
3) Face of control volume: regulates the separating surfaces between control volumes.
4) Grid lines: is to connect the two node points in neighbor.

One-dimensional example of computational grids for finite volume method is shown in Figure 3.3.
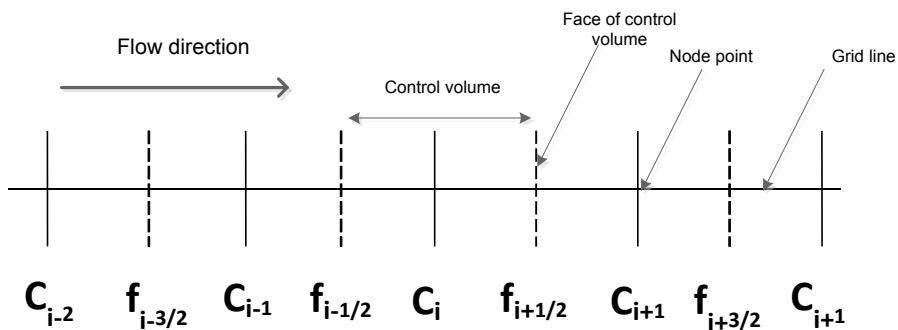

Figure 3.3 The computational grids of one-dimensional problem for finite volume method

In order to discretize the continuous governing equations, the discretization schemes are critical for implementation of the finite volume method. This indicates that the main problem of the finite volume method is the interpolation of the function values at the surface of the control volumes, because the solution is only available at the node points. Several commonly used discretized schemes are introduced below and their features are discussed. A simple and illustrative one-dimensional mass conservative model in Eq.(3.9) is selected to present different discretization schemes.

$$\frac{\partial c}{\partial t} + u \frac{\partial c}{\partial x} = 0 \tag{3.9}$$

This model describes a plug flow column. The outflow curve is monitored at the end of the column and is a function of time. This is an important and typical practice in chemical engineering, e.g. chromatographic and extraction columns which are discussed more in detail in publications [1] and [4]. In this example, a constant concentration pulse $c = 1.0 mol/l$ is introduced into the column. The column length is 1.0 meter. The flow rate in the column is 1.0 m/s. With these conditions, the analytical solution of the model is as in Figure 3.4.
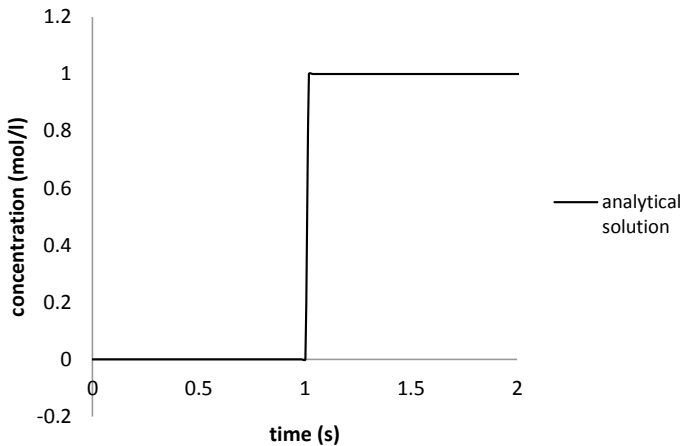

Figure 3.4 The analytical solution of the model in Eq.(3.9).

To solve the model in Eq.(3.9) with finite volume method, a number of discretization schemes are applied as presented below. Noticeably here, we select to use the method of lines, leaving the time variable continuous, and consider only the spatial discretization. The discretization form or partial discretization form of the model is:

$$\frac{\partial C}{\partial t} = -\frac{(uC_{i+\frac{1}{2}} - uC_{i-\frac{1}{2}})}{\Delta x_i} = -\frac{(f_{i+\frac{1}{2}} - f_{i-\frac{1}{2}})}{\Delta x_i} \tag{3.10}$$

f indicates the flux between different control volumes as in Figure 3.3. Different expressions of the flux represent different discretization schemes.

1) First order upwind scheme

The first order upwind scheme simply assumes that the value of the variables at the boundary equals to the value at the center of the control volume in upstream as (Hirsch, 1990):

$$f_{i+\frac{1}{2}} = C_i \tag{3.11}$$

As a low order method, the first order upwind scheme is stable and provides rational solutions in all conditions. Due to this reason, the scheme has been utilized widely and for long period. However similar with other low order methods, heavy numerical diffusion as shown in Figure 3.5, is an unavoidable disadvantage of the scheme.

2) Second order upwind scheme

In contrast to the first order upwind scheme, the second order upwind scheme uses two neighboring node points in upstream to estimate the value of the variables at the boundary as (Hirsch, 1990):

$$f_{i+\frac{1}{2}} = 1.5C_i - 0.5C_{i-1} \tag{3.12}$$

This is a second order scheme, classified already as a high order method. The accuracy of the solution is improved. Unfortunately the scheme generates numerical oscillations in the vicinity of steep gradients and discontinuities, explained by the Godunov's theorem (Wesseling, 2001) and shown in Figure 3.5.

3) QUICK scheme

QUICK scheme (Quadratic Upwind Interpolation of Convective Kinematics) is the 3rd order method. It considers three node points when estimating the value of the variables at the boundary as (Date, 2005):

$$f_{i+\frac{1}{2}} = \frac{6}{8}C_{i-1} + \frac{3}{8}C_i - \frac{1}{8}C_{i-2} \tag{3.13}$$

Similar with other high order methods, QUICK scheme generates also numerical oscillations as shown in Figure 3.5.

4) ENO and WENO schemes

In order to limit the numerical diffusion and oscillations to an accepted level, a number of methods have been developed such as high order method combined with flux limiters (Hirsch, 1990), and essentially non-oscillatory and weighted essentially non-oscillatory schemes (Harten et al., 1987). The idea behind these schemes is to simulate the smooth

curve with a high order scheme, but the shock curve with a low order scheme. However the disadvantage of application of flux limiters is that no particular flux limiter has been found to work well for all problems, and a particular choice is usually made on a trial and error basis (Sweby, 1984).

In ENO and WENO schemes, how to judge the smoothness, discontinuity or shock of the stencil mathematically is of great importance (Harten et al., 1987). ENO scheme is to keep the smoother stencil, but discard the less smooth stencil. WENO is to keep both the smoother stencil and the less smooth stencil, but give them different weighting coefficients. Details of the ENO and WENO schemes can be found in (Harten et al., 1987; Liu et al., 1994; Jiang & Shu, 1996).

In Figure 3.5, 3rd order WENO is applied. It can be seen that the solution performance is improved in respect of the limitations of numerical diffusion and numerical oscillations, compared to other schemes. In addition, if higher order of WENO is used (e.g. 5th order WENO), the result is expected even better than the above 3rd order WENO, but with increased computational load.
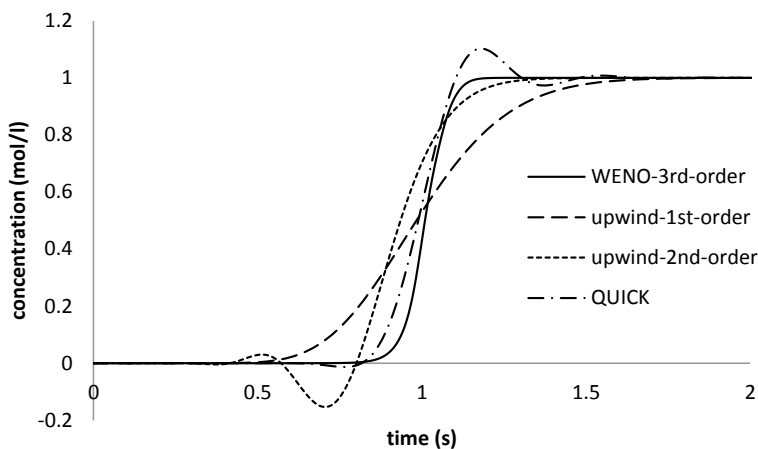

Figure 3.5 The simulation curves with first order upwind scheme, second order upwind scheme, QUICK and WENO.

In respect of the discretization, the finite volume method can be understood as the intermediate between the finite difference method and the finite element method. Finite difference method considers the variable development on the node points, but not the change between the node points. Finite element method considers only the changes between the node points (Reddy, 2005). Finite volume method intends to determine the values of the variables on the node points, which is similar with the finite difference method. In the finite volume method distribution must be assumed between the node points, similarly to the finite element method.

Finite volume method is usually categorized as a weighted residual method because it is in principle identical with the subdomain method. In implementation, the finite volume method and the finite difference method are very similar. However, for complex geometries in computational fluid dynamics, the finite volume method is more suitable than the finite difference method. As well, the finite volume method has an additional advantage of discretizing directly the conservation form of the governing equations. This implies that the discretized equations preserve the conservations laws better compared to e.g. the finite difference method of which the conservations laws are satisfied only approximately with very dense grids. It is sometimes possible to discretize the fluxes at the boundaries of the control volume by the finite difference method. In this case, the method has often been referred to as conservative finite difference method (Samarskii, 2001). The specificity of the finite volume method with respect to the finite difference method is that the discretization is performed on the local balance equations, rather than the PDE; the fluxes on boundaries of the control volumes are discretized, rather than the continuous differential operator.

3.4 Weighted Residual methods

In this section, the weighted residual methods are introduced. In (Finlayson, 1980) and (Fletcher, 1991), detailed discussions of the weighted residual methods can be found. The fundamentals of the weighted residual methods is that an approximation solution is assumed in the form of Eq.(3.14):

$$\Psi(z,t) \equiv \sum_{j=1}^{J} a_j(t)\phi_j(z) \tag{3.14}$$

$a_j(t)$ are the unknown coefficients and ϕ_j are the known analytical functions or trial functions, which may be e.g. polynomials or trigonometric functions. The number of the coefficients a_j is the method order. Here $F = 0$ is the governing equation to be solved. If the approximation solution in Eq.(3.14) is used to replace the exact solution in the governing equation F, a residual appears as:

$$F(\Psi) = R \tag{3.15}$$

The residual R is also a continuous function of z and t as in Eq.(3.14). The residual R approaches zero in the computational domain if the method order is sufficiently high and the unknown coefficients $a_j(t)$ are properly selected. The method to determine the values of $a_j(t)$ is to set the integral of the weighted residual in the computational domain as zero:

$$\int W_m(z)R(z)dz = 0 \tag{3.16}$$

Different formulations of the weighting function $W(z)$ denote different approaches in the category of weighted residual methods, which are explained further in the following sub-sections.

3.4.1 Subdomain method

The weighting function in the subdomain method is expressed as:

$W_m = 1$ in the computational subdomain

$W_m = 0$ out of the computational subdomain

According to the weighting functions in the computational subdomain, Eq.(3.16) becomes:

$$\int_a^b R(z)dz = 0 \tag{3.17}$$

This is exactly identical to the finite volume method as mentioned previously. Therefore the finite volume method is usually grouped in the weighted residual methods.

3.4.2 Least Squares Method

The weighting function of the least squares method is:

$$W_m(z) = \frac{\partial R}{\partial a_m} \tag{3.18}$$

Eq.(3.18) is equivalent to the requirement that $\int R^2(z)dz$ is to be minimized.

3.4.3 Collocation method

The weighting function is $W_m(z) = \delta(z - z_m)$, where δ is the Dirac delta function. δ is defined as $\delta = 1$ when $z = z_m$; $\delta = 0$ when $z \neq z_m$. All the points at $z = z_m$ are called collocation points. At the collocation points, the residual R is forced to be zero. In case the collocation points are considered as the node points of the finite difference method, the collocation method without the use of an approximation solution becomes very similar with the finite difference method.

In practical applications, the trial functions are usually or even exclusively selected as a series of orthogonal polynomials. The collocation points are the roots of an orthogonal polynomial, e.g. the roots of the Jacobi polynomial. It is then called as orthogonal collocation method, which is a particularly effective interpretation of the collocation method (Fletcher, 1991). The orthogonal collocation method is advantageous in implementation because it can be written in a compact matrix notation. The function values at the collocation points can be calculated conveniently. Special attention on the boundary condition is needed in implementation of the orthogonal collocation method because the boundary conditions are not automatically satisfied by the collocation equation. The solution is in fact straightforward that the collocation equations are written for the inner collocation points. The values of the two end points of the computational domain are solved to satisfy the boundary conditions, which is quite similar with the finite difference

method. To evaluate the performance of the collocation method in respect of computational accuracy, a rule of thumb is available (Rice & Do, 1995) as:

"normal polynomials + arbitrary collocation points" < "normal polynomials + roots of orthogonal polynomials as collocation points" < "orthogonal polynomials + roots of orthogonal polynomials as collocation points"

If the computational domain is divided into subdomains and the orthogonal collocation method is applied to each subdomain, then this method is called the orthogonal collocation method on finite elements. Orthogonal collocation and orthogonal collocation on finite element methods are attractive numerical tools for solving chemical engineering problems and have been widely used for decades. A number of the classical textbooks (Fletcher 1991, Finlayson 1972, Finlayson 1980, Rice & Do, 1995, Villadsen & Michelsen, 1978) focusing on computational techniques discuss the methods extensively. The orthogonal collocation method is particularly effective on one-dimensional parabolic partial differential equations. The most common application of the method is in reaction and diffusion problems (Finlayson 1980). For example a chromatographic general rate model was solved by the orthogonal collocation on finite element method (Gu et al., 1990).

3.4.4 Galerkin method

The idea behind the Galerkin method is the weighting function must be selected in the way which is similar with the trial function as:

$$W_m(z) = \phi_m(z) \tag{3.19}$$

For example, if the trial functions form a complete set (for polynomials a complete set would be $1, x, x^2, x^3, x^4, ...x^J$), Eq.(3.16) indicates that the residual is orthogonal to every member or a complete set. Consequently when J tends to infinity, the approximating solution converges to the exact solution (Fletcher, 1991).

The commonly used trial functions in the Galerkin method are linear or quadratic functions that are not zero in the computational domain. Figure 3.6 is a typical configuration of linear approximating functions.
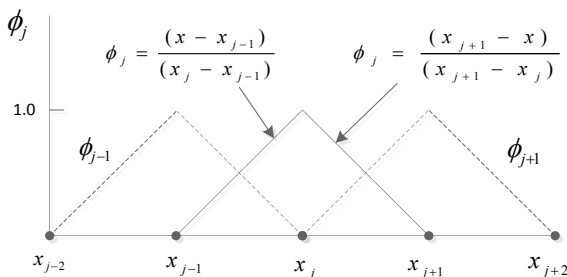
Figure 3.6 One-dimensional linear approximating functions. The domain between x_{j-1} and x_j is element A; between x_j and x_{j+1} is element B.

The Galerkin method is the foundation for a family of computational techniques called finite element methods (Fletcher, 1991), which emphasize the status of the Galerkin method.

3.4.5 Moment method

The moment method is one of the most important topics in this thesis. The key idea of the moment method is to follow the time evolution of the moments of the concentration profiles. Similar with the aforementioned methods in this section, the moment method can be introduced also with the notion of residuals. As can be seen in Section 4, the moment transformation procedure is presented based on the concept of residuals. Here instead, we introduce the moment method by the definition of moments. The j:th moment of a distribution is:

$$m_j = \int_0^1 \psi(\zeta)\zeta^j d\zeta \tag{3.20}$$

The derivative of moment m with respect to the dimensionless time θ is:

$$\frac{dm_j}{d\theta} = \frac{\partial}{\partial\theta} \int_0^1 \psi(\zeta)\zeta^j d\zeta \tag{3.21}$$

According to the Leibniz rule, the differential operator on the right hand side can be moved into the integral:

$$\frac{dm_j}{d\theta} = \int_0^1 \frac{\partial\psi(\zeta)}{\partial\theta}\zeta^j d\zeta \tag{3.22}$$

In the Publication [1-4], moment transformation of the model equations was carried out according to Eq.(3.22). The application details of the moment method will be introduced in more details in the following section.

4. Applications of the mass transfer and reaction models with the moment method

The general formulations of the model and the procedures to utilize the moment method are introduced in the beginning of this section. Hereafter detailed presentation is carried out in accordance with the subject of individual publication embedded in this thesis.

- One-dimensional mass transfer and reaction model

The models applied in this thesis contain in general two phases, 1) the bulk fluid phase; 2) the particle phase describing stagnant liquid and solid material in the particle. The mass transfer processes considered in the models are: 1) diffusion in the particle phase, 2) film mass transfer between the particle phase and the bulk fluid phase, 3) axial dispersion and convection in the bulk phase. The reactions are described as the source terms of the model. The model formulations are presented below.

Bulk fluid phase:

$$\frac{\partial C_{bi}}{\partial t} + u\frac{\partial C_{bi}}{\partial z} + \frac{3k_i(1-\varepsilon_b)(C_{bi} - C_{pi,R=R_p})}{\varepsilon_b R_p} - D_i\frac{\partial^2 C_{bi}}{\partial z^2} = S(C_b)_{reation} \tag{4.1}$$

Particle phase:

$$\frac{\partial C_{pi}}{\partial t} - \varepsilon_p D_{pi}\frac{1}{R^2}\frac{\partial}{\partial R}\left(R^2\frac{\partial C_{pi}}{\partial R}\right) = S(C_p)_{reation} \tag{4.2}$$

The first, second, third and fourth terms on the left hand side of Eq. (4.1) represent variation of bulk phase concentration against time, convection, mass transfer between the bulk and particle phases, and axial dispersion in the bulk phase, respectively. The first and second terms on the left hand side of Eq. (4.2) represent the variation of particle phase concentration against time, the diffusion in the particle phase. The terms on the right hand sides of Eq.(4.1) and (4.2) are the source terms. The models applied in Publications [1-4] and in this section are modified or extended from the model equations in Eq. (4.1) and (4.2). The initial and boundary conditions are presented subsequently when particular modeling cases are introduced. By introducing the dimensionless terms, Eq. (4.1) and (4.2) can be transformed into the dimensionless forms in Eq. (4.3) and (4.4). C_{ref} equals to the reference concentration of the component in question. More details about the initial and boundary conditions, as well as the derivations of dimensionless models can be found in Publications [1-4].

The dimensionless terms are:

$$\psi_b = \frac{C_b}{C_{ref}} , \ \psi_p = \frac{C_p}{C_{ref}} , \ \psi_p^s = \frac{C_p^s}{C_{ref}} , \ r = \frac{R}{R_P} , \ \zeta = \frac{z}{L} , \ \theta = \frac{ut}{L} , \ \mathrm{Pe} = \frac{uL}{D} , \mathrm{Bi} = \frac{kR_P}{\varepsilon_P D_P} ,$$

$$\eta = \frac{\varepsilon_P D_P L}{R_P^2 u} , \ \xi = \frac{3Bi\,\eta(1-\varepsilon_b)}{\varepsilon_b}$$

Dimensionless forms of Eq. (4.1) and (4.2) are:

Bulk phase:

$$\frac{\partial \psi_{bi}}{\partial \theta} + \frac{\partial \psi_{bi}}{\partial \zeta} + \xi_i(\psi_{bi} - \psi_{pi,r=1}) - \frac{1}{Pe_i}\frac{\partial^2 \psi_{bi}}{\partial \zeta^2} = s(\psi_b)_{reaction} \qquad (4.3)$$

Particle phase:

$$\frac{\partial \psi_{pi}}{\partial \theta} - \eta_i \frac{1}{r^2}\frac{\partial}{\partial r}\left(r^2 \frac{\partial \psi_{pi}}{\partial r}\right) = s(\psi_p)_{reaction} \qquad (4.4)$$

- Moment transformation

The moment method has been applied throughout Publications [1-4]. Based on the definition of moments in Eq.(3.20)-(3.22), moment transformations of the model equations were already introduced in Publication [1]. We derive here again the moment transformation form from the notion of the weighted residual methods, because the moment method is one of the members of the weighted residual methods. To do so, it could be seen clearly that the objective of the moment method is to minimize the errors of the moments of the modeled concentration profiles. The particle phase model equation is used here as an example to demonstrate the procedure of the moment transformation. Similar procedure of the moment transformation for the bulk phase model can be found in (Roininen, 2010).

Polynomial approximation as in Eq.(4.5), is used for the estimation of modeled particle-internal concentration profiles. Orthogonal polynomials that are functions of r^2 as (Finlayson, 1980) are selected since boundary condition ($\frac{dc}{dr} = 0$, at $r = 0$) requires that 1st order term is zero:

$$\psi_{pi}(r,\theta) = \sum_{i=1}^{n+1} w_i(\theta) r^{2i-2} \qquad (4.5)$$

When the particle-internal concentration profile is estimated by the polynomial approximation, the residual R appears as:

$$\frac{\partial \psi_{pi}}{\partial \theta} - \eta_i \frac{1}{r^2} \frac{\partial}{\partial r}\left(r^2 \frac{\partial \psi_{pi}}{\partial r}\right) - s_i(\theta,r)_{reaction} = R \qquad (4.6)$$

The coefficients $w_i(\theta)$ in Eq.(4.5) are determined by integrating the residual R over the computational domain as in Eq.(4.7) and setting this value to zero. Hence the errors of $w_i(\theta)$ can be minimized.

$$\int_0^1 R r^j dr = \int_0^1 \left(\frac{\partial \psi_{pi}}{\partial \theta} - \eta_i \frac{1}{r^2} \frac{\partial}{\partial r}\left(r^2 \frac{\partial \psi_{pi}}{\partial r}\right) - s_i(\theta,r)_{reaction}\right) r^j dr = 0 \qquad (4.7)$$

As integration is a linear operation, each term can be integrated separately. Rearranging Eq.(4.7) gives:

$$\int_0^1 \frac{\partial \psi_{pi}}{\partial \theta} r^j dr = \int_0^1 \left(\eta_i \frac{1}{r^2} \frac{\partial}{\partial r}\left(r^2 \frac{\partial \psi_{pi}}{\partial r}\right) + s_i(\theta,r)_{reaction}\right) r^j dr \qquad (4.8)$$

The left hand side of Eq.(4.8) is the definition of j:th moment. Therefore Eq.(4.8) becomes:

$$\frac{\partial m_{pi}^j}{\partial \theta} = \int_0^1 \left(\eta_i \frac{1}{r^2} \frac{\partial}{\partial r}\left(r^2 \frac{\partial \psi_{pi}}{\partial r}\right)\right) r^j dr + \int_0^1 s_i(\theta,r)_{reaction} r^j dr \qquad (4.9)$$

By inserting the appropriate boundary conditions, the moment transformation form is:

$$\frac{dm_{pi}^j}{d\theta} = \eta_i \left[\left.\frac{\partial \psi_{pi}}{\partial r}\right|_{r=1} - \int_0^1 \frac{\partial \psi_{pi}}{\partial r}(j-2)r^{j-1} dr\right] + \int_0^1 s_i(\theta,r)_{reaction} r^j dr \qquad (4.10)$$

The coefficients $w_i(\theta)$ are directly related to the concentration profile moments based on a linear transformation as:

$$(m) = [A](w) \qquad (4.11)$$

Where the elements of $[A]$ are:

$$A_{j,i} = \frac{1}{2i+j+1}, \qquad\qquad i = 1 \ldots n+1, \ \ j = 1 \ldots n+1 \qquad (4.12)$$

The weights $w_i(\theta)$ of Eq.(4.5) can be calculated from:

$$(w) = [A]^{-1}(m) \qquad (4.13)$$

Where $[A]^{-1}$ is the reverse matrix of $[A]$.

The transformation matrix depends only on selection of the polynomial and the number of moments. Thus the matrix for a selected polynomial does not depend on time related variables and can be constructed and inverted prior to the time integration of the model. This feature saves the CPU time considerably. Different polynomial trial functions and the according transformation matrixes were used throughout this study. Detailed introduction can be found in (Alopaeus, Laavi & Aittamaa, 2008) and Publication [1].

4.1 Moment method as a numerical tool for chromatographic general rate model

Moment method is applied in Publication [1] to solve the chromatographic general rate model. The chromatographic general rate model is modified from the mass transfer and reaction model in Eq.(4.1) and (4.2). Since no reactions occur in the chromatographic processes, as a result the reaction term is typically removed in the chromatographic general rate model. In addition, equilibrium between the solid part of the chromatographic resin particle and the stagnant liquid confined in the particle needs to be considered. Therefore the particle phase is divided into two parts, the solid particle and the stagnant liquid. The dimensionless model formulations are:

Bulk fluid phase:

$$\frac{\partial \psi_{bi}}{\partial \theta} = -\frac{\partial \psi_{bi}}{\partial \zeta} + \frac{1}{Pe_i}\frac{\partial^2 \psi_{bi}}{\partial \zeta^2} - \xi(\psi_{bi} - \psi_{Pi,r=1}) \tag{4.1.1}$$

Particle phase:

$$(1-\varepsilon_P)\frac{\partial \psi_{pi}^s}{\partial \theta} + \varepsilon_P \frac{\partial \psi_{pi}}{\partial \theta} = \eta_i \frac{1}{r^2}\frac{\partial}{\partial r}\left(r^2 \frac{\partial \psi_{pi}}{\partial r}\right) \tag{4.1.2}$$

The first term on the right hand side of Eq.(4.1.1) is the variation of bulk phase concentration against time. The first, second and third terms on the left hand side of Eq.(4.1.1) describe convection, mass transfer between the bulk and particle phases, and axial dispersion in the bulk phase, respectively. The first and second terms on the left hand side of Eq. (4.1.2) represent the solid material and the stagnant liquid of particle phase. The term on the right hand side of Eq.(4.1.2) depicts the diffusion in the particle phase.

The typical initial and boundary conditions for normal chromatographic operations:

I.C. $\theta = 0$, $\psi_{bi} = \psi_{bi}(0,\zeta)$; $\psi_{pi} = \psi_{pi}(0,r,\zeta)$ $\hspace{2cm}$ (4.1.3)

B.C. $\zeta = 0$, $\frac{\partial \psi_{bi}}{\partial \zeta} = Pe_i(\psi_{bi} - C_{f,i}(\theta)/C_{ref,i})$; $\zeta = 1$, $\frac{\partial \psi_{bi}}{\partial \zeta} = 0$ $\hspace{1cm}$ (4.1.4)

$$r = 0, \ \frac{\partial \psi_{pi}}{\partial r} = 0; \ r = 1, \frac{\partial \psi_{pi}}{\partial r} = Bi_i(\psi_{bi} - \psi_{pi,r=1}) \tag{4.1.5}$$

The initial conditions in Eq.(4.1.3) describe that no components exist in the bulk and particle phases at $\theta = 0$. The first term of the bulk phase boundary conditions in Eq.(4.1.4) indicates that a rectangular concentration pulse with the height of $C_{f,i}$, and the width of θ is introduced into the chromatographic column from its entrance ($\zeta = 0$). The second term of the particle phase boundary conditions in Eq.(4.1.5) depict the mass transfer between the particle and the bulk phases at the particle boundaries ($r = 1$).

4.1.1 Implementation procedure of the moment method

The moment transformation for the bulk fluid phase is similar as in previous publications (Alopaeus, Laavi & Aittamaa, 2008; Roininen & Alopaeus, 2011). For the particle phase, the model equations are coupled by the competitive isotherms written as:

$$\psi_{pi}^{s} = \frac{A_i \psi_{Pi}}{1 + \sum_{k=1}^{Nc}(B_k)\psi_{Pk}} \qquad \text{where } A_i = q_{s,i}b_i, \ B_k = b_k C_{0,k} \tag{4.1.6}$$

The moment transformation routine becomes different compared to solving the independent PDEs. The new moment transformation routine for the particle phase includes three steps: 1) the use of the new parameter G representing the average concentration in the particle phase; 2) the expression of $\frac{d\psi_p}{d\theta}$, representing the concentration derivative in the stagnant liquid in the particle phase, are solved from algebraic function pairs; 3) the moment transformation is done based on the expression of $\frac{d\psi_p}{d\theta}$ obtained from step 2). Detailed moment transformation forms for bulk fluid phase model and particle phase model can be found in Publication [1].

The idea of the moment method is to follow the time evolution of the concentration profile moments. The implementation procedure of the moment method is: 1) the model expression of $\frac{dC}{dt}$ is first transformed to $\frac{dm}{dt}$ via moment transformation; 2) The ODEs $\frac{dm}{dt}$ are solved by the solver (LSODE) to obtain the values of moments; 3) The weights are calculated by linear transformation from the moments; 4) The concentration profiles are calculated by polynomial approximation. This calculation routine is presented in a concise form as:

$$\frac{dC}{dt} \rightarrow \frac{dm}{dt} \rightarrow m \rightarrow w \rightarrow C \tag{4.1.7}$$

The calculation routine mentioned above can be also modified as:

$$\frac{dC}{dt} \rightarrow \frac{dm}{dt} \rightarrow \frac{dw}{dt} \rightarrow w \rightarrow C \tag{4.1.8}$$

This indicates that time derivative of the weights are used as the integrated variables instead of the moments. Time derivative of the weights is calculated by means of $\frac{dw}{dt} = [A]^{-1}\frac{dm}{dt}$. Based on this modified routine, the concentration can be calculated at each time step directly from the weights of the selected polynomial. This is faster than to calculate the concentration each time from moments to weights to concentration with the original routine. In this study, integration has been always implemented on $\frac{dw}{dt}$, not $\frac{dm}{dt}$ in

order to decrease the computational load. The shortened CPU time is presented in Table 1 of Publication [1] as an example.

4.1.2 Numerical parameters of the moment method

Two important ways can be applied to improve the accuracy of the moment method. One is to increase the degree of the polynomials which approximate the concentration profiles. The other is to divide the whole computational domain into a number of subdomains. In Publication [1], detailed discussions can be found for the effects of numerical parameters. In the works of Publication [1] and [2], the degree of the polynomials were third and second in the bulk phase and in the particle phase respectively. The whole computational domain in the bulk phase was divided into 12 subdomains.

4.1.3 Algorithm verification and experimental simulations

In order to verify the computational accuracy of the moment method, mass balance of the model is investigated first. In addition, the concentration profiles solved by the moment method are compared with an applicable analytical solution. In the end, the modeled profiles are compared with the measured results in order to verify the applicability of the moment method as well as the general rate model.

- Mass balance verifications

Mass balance investigation is an important and effective tool to discover implementation errors and to ensure the accuracy of the simulated results. In this work, comparison is made between the numerical area under the simulated profile and the theoretical mass input. A number of test cases are carried out to check the mass balance. In all the tests, the errors were below 0.3%. More detailed results for mass balance check can be found in Table 1 of Publication [1].

- Comparison with an analytical solution

Comparison with an analytical solution is also an effective tool to verify the numerical solution method. However in this work, the general rate model and the competitive isotherms are complicated, its analytical solution is not available in literature. In a recent publication (Siitonen & Sainio, 2011), the explicit equations for the height and position of the first component shock for binary mixtures with competitive Langmuir isotherms under ideal conditions (no mass transfer resistance and no axial dispersion) were developed. Together with the previously published results of Golshan-Shirazi and Guiochon (Golshan-Shirazi & Guiochon, 1989; Golshan-Shirazi & Guiochon, 1989), the analytical solution for the entire chromatographic outflow curves can be obtained. Our numerical solution is compared with the analytical solution as presented in Figure 4.1.1. The dimensionless isotherm parameters [A, B] for component 1 and 2 are [2.0, 0.2] and [2.5, 0.25] respectively as in Eq.(4.1.6). The dimensionless injection volume is 0.17 for both components. It can be seen that the numerical solution and the analytical solution are reasonably close to each other. Further, the retention times of the two shocks are correct. This result suggests that the moment method is implemented correctly.
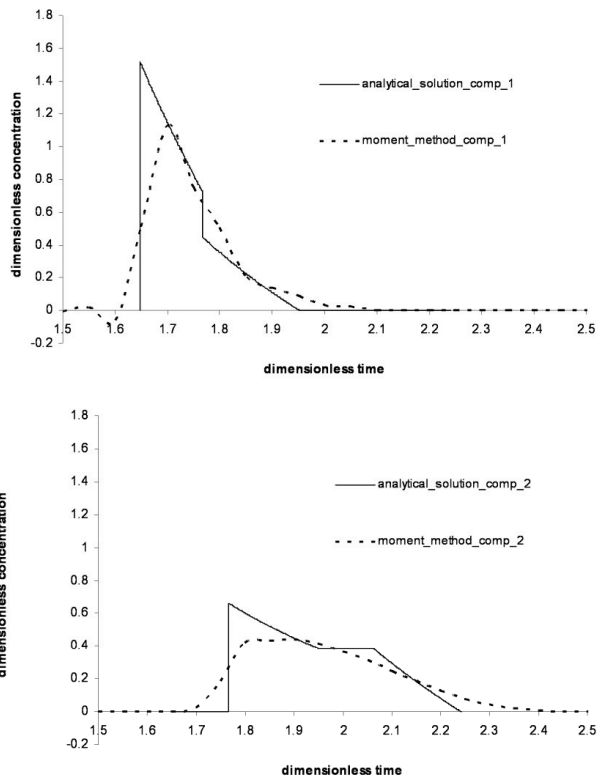
Figure 4.1.1. Comparison between analytical solution (solid lines) under ideal condition and moment method numerical solution (dotted lines) with mass transfer resistance. The analytical solution of components 1 and 2 are shown respectively.

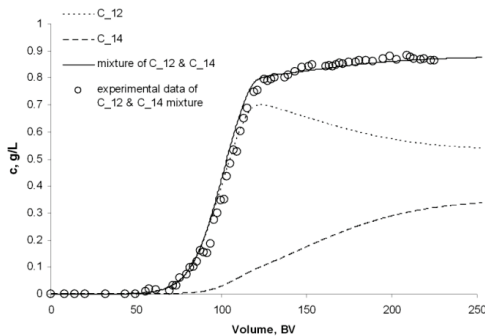*- Simulation of benzalkonium chloride adsorption*

The comparison between the experimental and simulated results for the verification of the model and the numerical scheme is a common practice. The experiment of adsorptive removal of benzalkonium chloride from water in an adsorption column (Turku & Sainio, 2009) is used for the purpose of verification in this work. The experiment was about the adsorption of C12 and C14 homologues of benzalkonium chloride from water. The bed porosity was ε_b=0.46. The particle porosity was ε_p=0.60. Effective particle radius was 0.53 mm. Total feed concentration was 0.87 g/L. Feed composition was 60% C12 and 40% C14. Flow rate was 1.66×10^{-5} ms^{-1} or 2 BV/h. Column inner diameter was 1.6 cm. The bed volume was 6 ml. Detailed experimental parameters can be found in the reference (Turku & Sainio, 2009).

The applied nonlinear competitive Langmuir isotherm was:

$$q_j = \frac{q_{s,j} b_j C_j^L}{1 + \sum_{k=1}^{2} b_k C_k^L}, j = 1,2 \tag{4.1.9}$$

q_s for C12 and C14 are 1.13 and 1.35 molL^{-1}; b for C12 and C14 are 2381.2 and 4531.3L mol^{-1}. Other model parameters include: Axial dispersion coefficient is $D_{ax} = 5.4 \times 10^{-8}$m^2 s^{-1} for all components; The liquid film mass transfer coefficient $k = 4.5 \times 10^{-7}$ ms^{-1} is used for C12 and C14; The pore diffusion coefficients for C12 and C14 are 1.0×10^{-10} and 1.4×10^{-10} m^2 s^{-1} respectively. (Turku & Sainio, 2009)

From modeling point of view, adsorption is identical with chromatography. Therefore the general rate model for chromatographic column introduced can be used directly to simulate the adsorption process. In the experiment, only the total concentration of C12 and C14 homologues was able to be measured (Turku & Sainio, 2009), thus the experimental (circles) and simulated (solild line) total concentrations were used for comparison in Figure 4.1.2. Dashed lines represent the simulated outlet concentrations for the individual homologues. It can be seen that the simulated curve is in conformity with the measured result. The applicabilities of the moment method and the general rate model predict are verified.

Figure 4.1.2. Benzalkonium chloride experimental data (circles) and simulated curves (lines)

Worthwhile to mention, the moment method has been frequently verified with another numerical method, orthogonal collocation and finite element method during the development of the simulator, which was provided by Gu (Gu et al., 1990). Identical results were observed in all test cases from these two numerical methods.

4.2 Estimation of chromatographic general rate model parameters with the moment analysis method

In Publication [2], the moment values of the simulated chromatograms are applied for the estimation of the parameters in the chromatographic general rate model. The model applied in this work is identical with Publication [1], except the nonlinear Langmuir isotherm as $\psi_{p,r=1} = \dfrac{a\psi_b}{1+b\psi_b}$ is used, instead of the nonlinear competitive isotherm. Three characteristic values of a curve are utilized in the parameter optimization process of this work. The values of the curve are the mean μ, the standard deviation σ and the skewness γ. These values are defined based on the first three moments of the curve, which are namely the first normalized moment, and second and third central moments. Definitions of the moments and the characteristic values are presented as below.

The first normalized moment (M_1), denoted also as μ, is the mean of the curve. For a chromatographic effluent curve, the discrete form of the first normalized moment is:

$$\mu = M_1 = \frac{\sum\limits_{i=1}^{k} C(t_i) t_i \Delta t_i}{\sum\limits_{i=1}^{k} C(t_i) \Delta t_i} \tag{4.2.1}$$

k is the total number of the experimental concentration points or the simulated concentration points. t_i is the sampling time. Δt_i is the time interval over which C is assumed to be $C(t_i)$.

The discrete form of second central moment (M_2) is:

$$M_2 = \frac{\sum\limits_{i=1}^{k} C(t_i)(t_i - \mu)^2 \Delta t_i}{\sum\limits_{i=1}^{k} C(t_i) \Delta t_i} \tag{4.2.2}$$

Its square root is the standard deviation σ:

$$\sigma = \sqrt{M_2} \tag{4.2.3}$$

The discrete form of third central moment (M_3) is:

$$M_3 = \frac{\sum\limits_{i=1}^{k} C(t_i)(t_i - \mu)^3 \Delta t_i}{\sum\limits_{i=1}^{k} C(t_i)\Delta t_i} \qquad (4.2.4)$$

The skewness γ, defined based on the third moment and the standard deviation is:

$$\gamma = \frac{M_3}{\sigma^3} \qquad (4.2.5)$$

For chromatography, retention time (related to the first moment), physical dispersion (related to the second moment) and skewness (related to the third moment) are the three most relevant characteristic values of the in-column chromatogram. The implementation principle of the moment method is to minimize the errors of moments in the in-column chromatogram. This suggests naturally that the three characteristic values of the in-column chromatogram are estimated with minimized errors. Thus the estimations of retention time, physical dispersion and skewness of the simulated effluent curve are also expected to be with good accuracy. In Figure 4.2.1, the simulated in-column chromatogram and the simulated effluent curve are presented to clarify their difference. Due to this feature, the moment method is advantageous compared to other numerical schemes for chromatographic simulations. Also based on this feature, a number of parameters of the chromatographic model are optimized with the utilization of these three characteristic values of the effluent curve in this work.
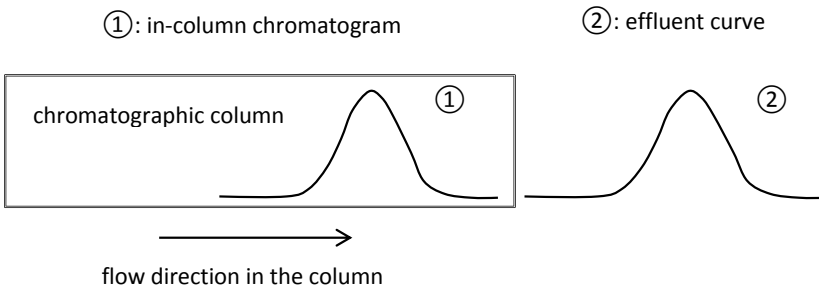
Figure 4.2.1. Graphic description of the simulated in-column chromatogram and effluent curve.

In order to show quantitatively that the effluent curve moments are predicted with "good accuracy" by the moment method, we compared against the analytical solution of retention time and physical dispersion of the effluent curve (Miyabe, 2008). The error-in-%, when compared with the analytical solution, are approximately within $\pm 0.05\%$ for retention time and $\pm 0.4\%$ for physical dispersion. As mentioned in Section 4.1, the degrees of the approximating polynomials in the bulk phase and in the particle phase here are third and

second, respectively. The whole computational domain in the bulk phase is divided into 12 subdomains. It can be seen that satisfactory results are obtained with these rather low number of variables, although the errors could be reduced further by using higher number of variables. The parameters and results in detail can be found in the following Table 4.2.1.

Table 4.2.1. Parameters and test results for comparison between the effluent curve moment values calculated analytically and the values by the moment method.

test No.	1	2	3	4	5	6
sample size(m3)	0.01	0.01	0.01	0.01	0.01	0.01
flow vol (m3/s)	8.0×10^{-6}	8.0×10^{-6}	8.0×10^{-6}	8.0×10^{-6}	8.0×10^{-6}	8.0×10^{-6}
diameter (m)	0.225	0.225	0.225	0.225	0.225	0.225
column length(m)	5.0	5.0	5.0	5.0	5.0	5.0
bed porosity	0.34	0.34	0.34	0.34	0.4	0.4
particle porosity	0.4	0.4	0.4	0.4	0.6	0.6
Dax (m2/s)	7.0×10^{-6}	6.0×10^{-6}	6.0×10^{-6}	7.0×10^{-6}	8.0×10^{-6}	8.0×10^{-6}
Dp (m2/s)	5.0×10^{-9}	6.0×10^{-9}	7.0×10^{-9}	5.2×10^{-9}	9.0×10^{-9}	9.5×10^{-9}
k (m/s)	1.8×10^{-5}	1.8×10^{-5}	1.8×10^{-5}	1.8×10^{-5}	1.8×10^{-5}	1.8×10^{-5}
Rp (m)	1.65×10^{-4}	1.65×10^{-4}	1.65×10^{-4}	1.65×10^{-4}	1.65×10^{-4}	1.65×10^{-4}
C0 (mol/l)	0.1	0.1	0.2	0.2	0.1	0.2
equilirium constant	1.08	1.1	1.2	1.24	1.3	1.5
retention time						
analytical solution	26262.75	26459.56	27443.64	27837.27	27264.72	28457.54
moment method	26273.56	26472.86	27455.98	27843.40	27259.19	28464.21
error	0.04%	0.05%	0.04%	0.02%	-0.02%	0.02%
physical dispersion						
analytical solution	3363379	2960785	3183555	3780106	4858247	5302706
moment method	3372687	2970275	3191491	3790052	4839065	5283989
error	0.28%	0.32%	0.25%	0.26%	-0.39%	-0.35%

Three issues need to be emphasized here when compared with analytical solutions of the 2 effluent curve moments.

1) In this comparison, linear isotherm was applied. This is because only with the simple linear isotherm, the analytical solution is available. No analytical solution can be found in the literature if the complicated nonlinear isotherm is used.

2) The model in Miyabe's paper (Miyabe, 2008) is slightly different from the model we used in this work. Miyabe's model intends to consider the effect of adsorption on the total mass transfer rate. But for our model the adsorption rate is infinitely fast because it is assumed that local equilibrium exists for each component between the pore surface and the stagnant fluid phase in the macro pores. Thus the adsorption term in Miyabe's model is removed when calculating the analytical solutions of the moment values, in order that our numerical solutions are comparable with the analytical solutions.

3) The analytical solution of the skewness (related to 3rd moment) is not available in open literatures. We cannot compare it in the same way as the retention time and physical dispersion. In this work, the skewness is used in the objective function for parameter fitting against the experimental data. The curves produced with the fitted parameters are very close to the experimental data with certain skewness. This indicates that the skewness can also be estimated by the moment method with good accuracy.

In this work, the unknown parameters are regressed against the experimental data (Saari et al., 55, 2010), in which the effluent curves of the chromatographic separation for glucose and galactose were measured. The fitting procedure optimizes the values of the model parameters by minimizing the residual sum of squares between experimental and simulated values for each set of single solute data in the effluent curves. The fitted parameters include pore diffusion coefficient D_p; isotherm parameter a and b for nonlinear

Langmuir isotherm $\psi_{p,r=1} = \dfrac{a\psi_b}{1+b\psi_b}$. Other simulation parameters and the starting values of

pore diffusion coefficients are estimated by the empirical formulations in literature (Chung and Wen, 1968; Mackie et al., 1955; Wilson et al., 1966). The starting values of the isotherm a and b are estimated from the experimental data.

Two objective functions were used in the fitting as in Eq.(4.2.5) and (4.2.6). The fitting made with Eq.(4.2.5) is called "moment fitting" which is to minimize the errors between the moments of the modeled curves and the moments of experimental data.

$$residual = w_1\left(\frac{\mu_S - \mu_E}{\mu_E}\right)^2 + w_2\left(\frac{\sigma_S - \sigma_E}{\sigma_E}\right)^2 + w_3\left(\frac{\gamma_S - \gamma_E}{\gamma_E}\right)^2 \qquad (4.2.5)$$

Where w is the weighting factor of each term; Subscript "S" represents the simulated curve and "E" represents the experimental curve.

The fitting by the objective function in Eq.(4.2.6) is called "concentration fitting", which focuses on the error minimization on each individual measured concentration point against the simulated values.

$$residual = \sum_{i=1}^{n}\left[f_i(t) - y_i(t)\right]^2 \qquad (4.2.6)$$

Where $y_i(t)$ is the concentration value (g/100ml) for one component at ith measurement point (at time t) measured in the experiment; $f_i(t)$ is the concentration value (g/100ml) for one component estimated by the model (also at time t); t is time (s) for different measurement points; n is total measurement points in the experiment.
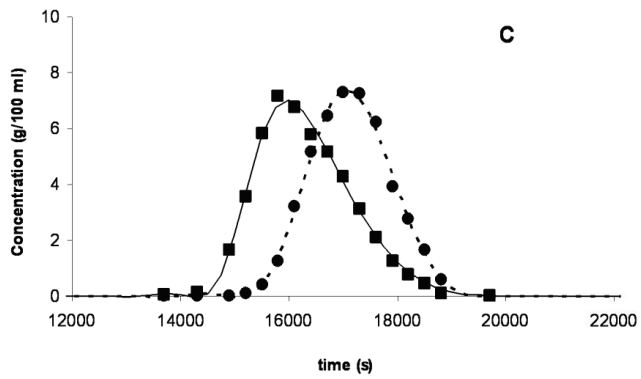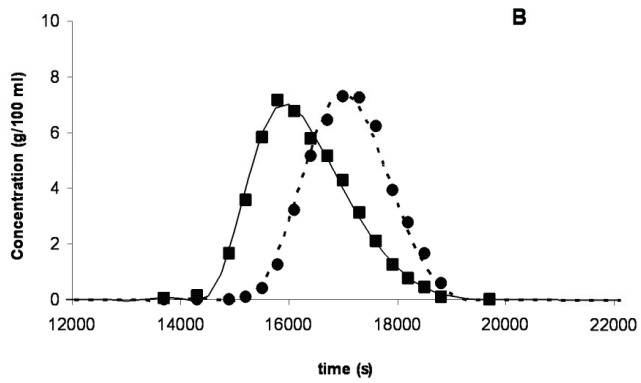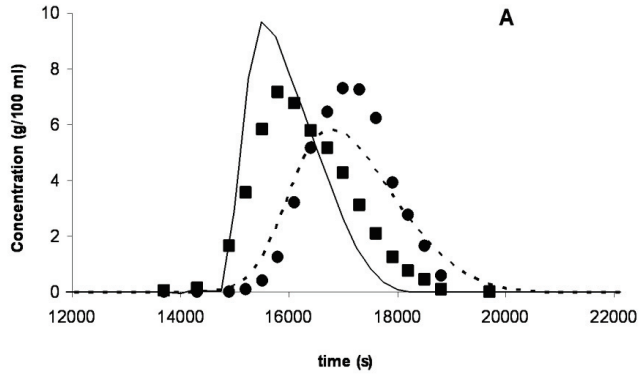
Three simulation cases and the used parameters were presented in Table 4.2.2 and Figure 4.2.2 (from Publication [2]). In Case A, all the parameters were calculated from empirical formulations. Deviation exists between the simulated profiles and the measured

curves as shown in Figure 4.2.2. In Case B, the "moment fitting" was used to determine the pore diffusion coefficient D_p and isotherm parameters a and b. The conformity between the modeled and measured curves is high as shown in Figure 4.2.2, B. In Case C, the "concentration fitting" was used instead to fit the pore diffusion coefficient D_p and isotherm parameter a and b. The modeled and measured curves are in good conformity as shown in Figure 4.2.2, C. It can be seen in Table 4.2.2 that the CPU time consumed for the "moment fitting" is considerably shorter than "concentration fitting". We also noticed that for "concentration fitting", the fitting is very sensitive to the selection of the initial values of the fitted parameters. It means that when the initial values are not reasonably close to the target values, the fitting process may fail. But for "moment fitting", this does not appear to be a problem and the parameters still can be optimized successfully. This feature of the "moment fitting" can be considered as an advantage over the "concentration fitting".

The merits of the moment analysis method in this study against the analytical solution of the moments include: 1) the moment values of the chromatograms can be calculated for more complicated isotherms, e.g. nonlinear competitive isotherms. For the moment values obtained by the analytical solutions, only the simple linear isotherm can be applied; 2) higher order moment values with good accuracy can be calculated from the simulated chromatograms. However, the analytical expressions are available for the first and second moments only, not for higher order moment values.

Table 4.2.2. Glucose and galactose chromatographic separation simulation parameters. Case A: no parameter fitting. Case B: moment fitting (All the weighting factors are 1.0). Case C: concentration fitting. Case D shows the moment values of the experimental data. The percentage values of mean, S.D. and skewness are the deviation rate from experimental data. The computer applied in this study is with Intel® Core™2 Duo CPU E7500 @ 2.93GHz.

a	b	Dp(m2/s)	concentration residual	mean (μ)		S.D. (σ)		skewness (γ)		CPU time (h)
Initial Values										
1.08	1.0×10^{-2}	5.78×10^{-10}	35.497	15964.4	-1.92%	628.2	-26.42%	0.5972	13.59%	-
1.24	1.0×10^{-2}	5.02×10^{-11}	15.630	17123.9	0.23%	964.8	34.86%	0.4620	346.69%	-
Moment Fitting										
1.126	1.150×10^{-2}	7.024×10^{-11}	0.702	16283.3	0.04%	853.6	-0.03%	0.5261	0.07%	2.2
1.171	8.230×10^{-4}	1.345×10^{-10}	1.691	17071.1	-0.08%	714.8	-0.08%	0.1038	0.31%	0.5
Concentration Fitting										
1.132	1.146×10^{-2}	7.014×10^{-11}	0.440	16322.5	0.28%	855.4	0.17%	0.5251	-0.12%	10.0
1.182	8.191×10^{-4}	1.340×10^{-10}	0.450	17143.6	0.34%	712.1	-0.46%	0.1039	0.43%	8.5
Moment Values of Experimental Data										
-	-	-	-	16277.4		853.9		0.5257		-
-	-	-	-	17085.5		715.4		0.1034		-

Figure 4.2.2. Glucose and galactose simulated effluent curves (lines) and experimental data (symbols). A: simulation before parameter fitting; B: simulation after moment fitting; C: simulation after concentration fitting

4.3 Modeling of mass transfer and reactions in anisotropic biomass particles

In Publication [3], the aim is to reduce the heavy computational load when the concentration profiles are solved inside anisotropic biomass particles. In this study, the rectangular wood chips are selected to represent biomass particles. The reasons for this selection are: 1) the wood chips, are very widely used as the raw material in different fields e.g. kraft pulping, biorefinery etc; 2) the kinetic models of wood chips are comparatively well developed. As shown in Figure 4.3.1, wood chips are usually immersed in water solution during the industrial processes, e.g. pulping, biorefinery etc, the mass transfer and reactions in the wood chips are considered and modeled in water phase.
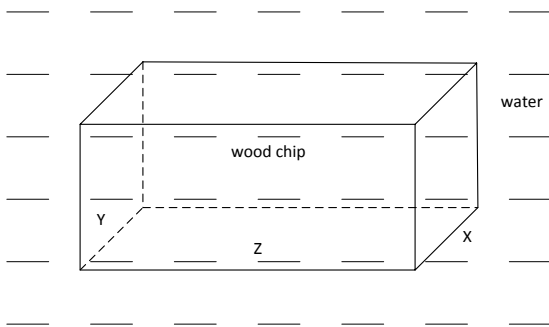

Figure 4.3.1. Illustrative picture of the wood chip in water. X,Y,and Z are the dimensions of the wood chip.

Due to the anisotropic properties of the wood chips, usually three dimensional (3D) models have been applied in order to consider the mass transfer phenomena accurately (Jutila, 1980; Grénman et al., 2010). The computational time to solve the complicated 3D models usually can be considerably long, especially if these are used with unit operation models. In this work, firstly we reduce the rigorous 3D model to one-dimensional (1D) model by introducing the geometrical shape parameter, which describes the rectangular shape of the wood chips. Secondly the high order moment method, instead of the conventionally used low order finite different method, is used in order to decrease further the number of variables with reduced computational load.

Three different models are utilized to describe the mass transfer and reactions in the anisotropic wood chips as: 1) the rigorous 3D model, considering different mass transfer resistance in all three directions; 2) the homogeneously mixed chip model (HMC model), in which the concentration profiles inside the particle are ignored, suggesting that the phase inside the particle is homogeneously mixed and all the mass transfer resistances are lumped into the film on the particle surface; 3) the 1D model as a reduced form of the 3D model, which is the main study objective in this work. The formulations of the three models are presented as below.

4.3.1 3D particle phase model

The 3D model accounts for different mass transfer resistance in all three dimensions.

The model of the wood chip phase is:

$$\frac{dC_i}{dt} = D_i \left[E_x' \frac{d^2 C_i}{dx^2} + E_y' \frac{d^2 C_i}{dy^2} + E_z' \frac{d^2 C_i}{dz^2} \right] + S_r \qquad (4.3.1)$$

The boundary conditions at the center of the chip as Eq.(4.3.2) and at the surface of the chip as Eq.(4.3.3) are:

$$x = y = z = 0 \,; \frac{dC_i}{dx} = \frac{dC_i}{dy} = \frac{dC_i}{dz} = 0 \qquad (4.3.2)$$

$$x = X, \frac{\partial C_i}{\partial x} = \frac{k_i \tau_{yz}}{\varepsilon_{yz} D_i} \left(C_{bi} - C_{i,x=X} \right); y = Y, \frac{\partial C_i}{\partial y} = \frac{k_i \tau_{xz}}{\varepsilon_{xz} D_i} \left(C_{bi} - C_{i,y=Y} \right);$$

$$z = Z, \frac{\partial C_i}{\partial z} = \frac{k_i \tau_{xy}}{\varepsilon_{xy} D_i} \left(C_{bi} - C_{i,z=Z} \right); \qquad (4.3.3)$$

Where D_i is the diffusion coefficient in water; E' is the Effective Capillary Cross Sectional Area for different directions as:

$$E_x' = \frac{\varepsilon_{yz}}{\varepsilon_p \tau_{yz}}, \ E_y' = \frac{\varepsilon_{xz}}{\varepsilon_p \tau_{xz}}, \ E_z' = \frac{\varepsilon_{xy}}{\varepsilon_p \tau_{xy}} \qquad (4.3.4)$$

In all the models of this study, S_r represents the reaction term $C + W \Rightarrow P$ with the reaction rate law $S_r = K_r C_c C_w$. C represents the inorganic reactant, *e.g.* alkali; W represents the lignin existing in the wood chips; P represents the product of the reaction, *e.g.* the dissolved lignin.

4.3.2 HMC particle phase model

In the Homogeneously Mixed Chip phase model (HMC), the concentration profiles inside the particle are ignored. This indicates that the phase inside the particle is assumed to be homogenously mixed and all the mass transfer resistances are lumped into the film on the particle surface. The HMC model formulation is:

$$\frac{dC_i}{dt} = \frac{1}{\varepsilon_p V_p} \left[k_{i,xy} \varepsilon_{xy} (C_{bi} - C_i) A_{xy} + k_{i,xz} \varepsilon_{xz} (C_{bi} - C_i) A_{xz} + k_{i,yz} \varepsilon_{yz} (C_{bi} - C_i) A_{yz} \right] + S_r \qquad (4.3.5)$$

where k_{xy}, k_{xz}, k_{yz} are the lumped mass transfer resistance coefficients in three directions of the wood chip; A_{xy}, A_{xz}, A_{yz} are the areas at different directions; ε_{xy}, ε_{xz}, ε_{yz} are the porosity at different directions; C_b is the bulk phase concentration.

4.3.3 1D particle phase model

The 1D model is a dimensional reduction of the 3D model with the formulation as:

$$\frac{\partial C_i}{\partial t} = \frac{D_i}{\tau} \frac{1}{R^{\Omega}} \frac{\partial}{\partial R} \left(R^{\Omega} \frac{\partial C_i}{\partial R} \right) + S_r \tag{4.3.6}$$

The initial and boundary conditions as:

$$t = 0, \ C = \begin{bmatrix} C_C & C_P & C_W \end{bmatrix}; \ R = 0, \ \frac{\partial C_i}{\partial R} = 0; \ R = L, \ \frac{\partial C_i}{\partial R} = \frac{k_i \tau}{\varepsilon_p D_i} \left(C_{bi} - C_{i,R=L} \right); \tag{4.3.7}$$

Where τ is the particle tortuosity; R is the particle characteristic dimension; Ω is the geometrical shape parameter which is defined as (Burghardt and Kubaczka, 1996):

$$\Omega = \frac{A_{\alpha}}{V_{\alpha}} L - 1 \tag{4.3.8}$$

A_{α} is the computational surface area of the particle and V_{α} is the computational volume of the particle. L equals to the smallest dimension of the wood chip divided by two. With proper choice for Ω, the equation can be used for slab ($\Omega = 0$), cylinder ($\Omega = 1$), and sphere ($\Omega = 2$). Detailed discussion about the geometrical shape parameter Ω can be found in Publication [3].

In this work the simulation profiles of the 3D model solved by the finite difference method are used as the reference, which are compared with the profiles of the HMC model and 1D model solved by the finite difference method or moment method. In the implementation to solve the 3D model, the concentration profiles of 1/8 of a rectangular wood chip are solved. The complete profile in the whole wood chip is obtained by the symmetric feature of the rectangular chip. The 3D model is solved by the finite difference method with nine grid points in each direction. As a result, the total number of grid points used to solve the model is 9 × 9 × 9. In the HMC model, only one variable is solved because the concentration inside the particle is considered uniform. In the 1D model by the finite difference method, 9 grid points are selected to guarantee the computational accuracy. To solve the 1D model with the moment method, for each component, 0th, 1st, and 2nd moment are conserved resulting in 3 variables. The polynomial functions selected is identical as Eq.(4.5). Detailed

discussion of the moment method to solve the 1D model can be found in Publication [3]. For 3D model and 1D model, the concentration profiles presented in the following figures are the average values calculated from the modeled concentration profiles. For HMC model, the concentration profile is directly the solved variable.

It can be seen in Figure 4.3.2 that the simulation profiles of HMC model are different from the 3D model. This indicates that ignoring the concentration profiles inside the chips may result in serious errors in the predicted compositions. In Figure 4.3.3, the simulated profiles of the 1D model solved by the finite difference method are in good conformity with the 3D model. Similarly the 1D model solved by the moment method provides also satisfactory consistency against the 3D model as in Figure 4.3.3. This suggests that the slightly compromised accuracy in 1D models results from the geometric assumption, not from various numerical methods. In Table 4.3.1, it can be seen clearly that the number of variables in the 3D model decreases dramatically in the 1D model solved by the finite difference method. The number of variables decreases further when the 1D model is solved by the moment method. This indicates that the 3D model is very time consuming to be solved. The high order moment method reaches similar accuracy with less number of variables and reduced computational load, compared to the low order finite difference method.
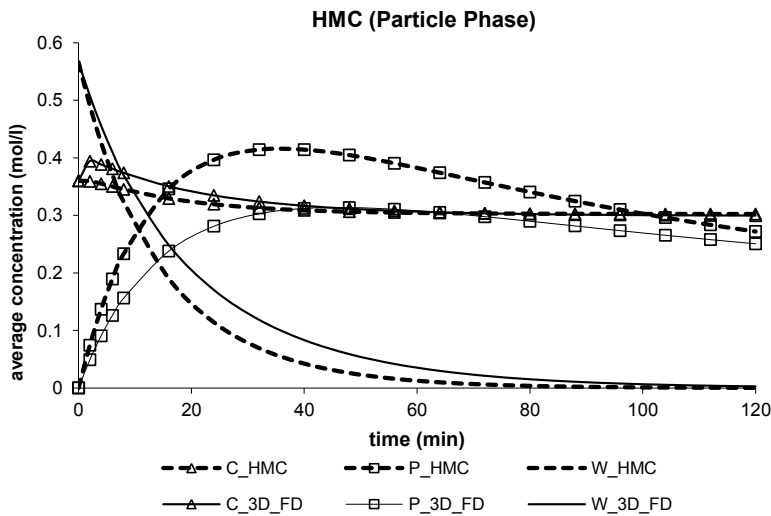

Figure 4.3.2. Average concentrations as a function of time in the particle phase. Dashed lines are the Homogeneously Mixed Chip phase model (HMC). Solid lines are the 3-D model with the finite difference method (3D_FD).
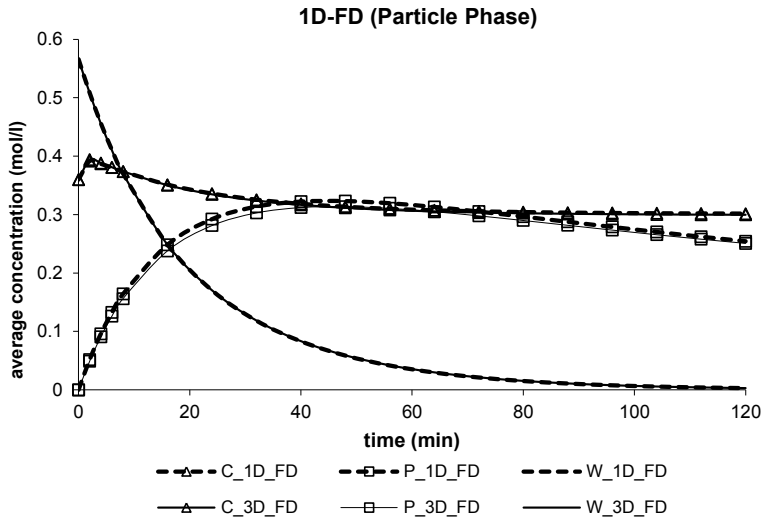
1D-FD (Particle Phase)

Figure 4.3.3. Average concentrations as a function of time in the particle phase. Dashed lines are the 1-D model solved with the finite difference method (1D_FD). Solid lines are the 3-D model with the finite difference method (3D_FD).
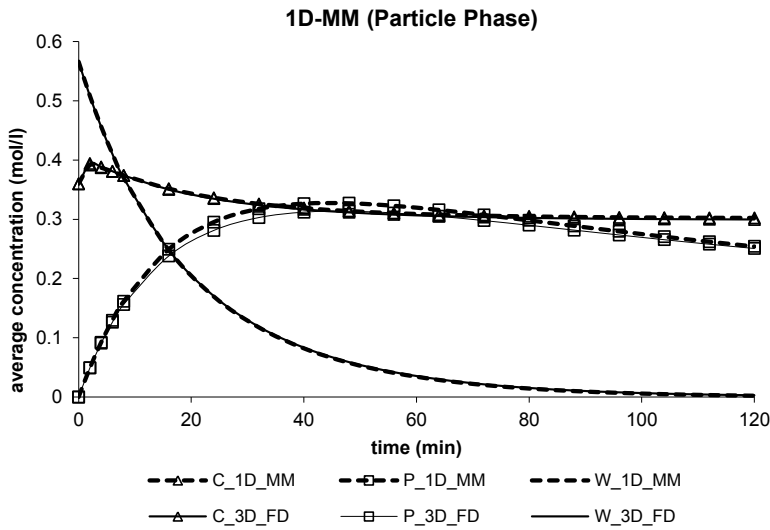

1D-MM (Particle Phase)

Figure 4.3.4. Average concentrations as a function of time in the particle phase. Dashed lines are the 1-D model with the moment method (1D_MM). Solid lines are the 3-D model with the finite difference method (3D_FD).

Table 4.3.1. Performance of various models and numerical schemes. Dev is the average quantitative deviation from the 3-D model; A-re and H-re are the average relative error and the highest relative error of individual point.

model	numerical method	accuracy	variables	CPU time(s)	Dev	A-re	H-re
3-D model	Finite Difference Method	-	9x9x9	96.1	-	-	-
HMC model	-	Bad	1	0.04	1.37×10^{-1}	3.0-40.0%	50.0%
1-D model	Finite Difference Method	Satisfatory	9	2.4	7.87×10^{-3}	3.0%	5.6%
1-D model	Moment Method	Satisfatory	3	0.3	8.29×10^{-3}	3.0%	6.0%

*The computer applied in this study is with Intel® Xeon® CPU E31230 @ 3.20GHz. Detailed definitions of Dev, A-re and H-re can be found in Publication [3].

4.4 Modeling of mass transfer and degradation of hemicelluloses in flow-through hot water extraction

One important objective of hot water extraction process is to separate hemicelluloses from wood. The topic of Publication [4] is to present a model which simulates the average molecular weights and the outflow mass of the extracts in flow-through hot water extraction process. Three phases and four mass transfer phenomena are considered in this model. Three phases are: 1) bulk liquid phase, 2) stagnant liquid phase in the voids of the wood particles, and 3) the solid wood particle phase. Four mass transfer phenomena are: 1) dissolution of the polymers from the solid wood particle phase, 2) diffusion of the polymers in the stagnant liquid phase, 3) film mass transfer between the stagnant liquid phase and the bulk liquid phase, 4) axial dispersion of the polymers in the bulk phase. The model is modified and extended from the one-dimensional mass transfer and reaction model of Eq.(4.1) and (4.2). Because the hemicellulose polymers dissolute from the solid wood particle to the stagnant liquid confined in the pores of wood particles, the particle phase model in Eq.(4.2) is reformulated into two phase equations, namely stagnant liquid phase and solid wood particle phase. By doing so, mass transfer between the two phases can be described appropriately. In addition, degradation of the hemicellulose polymers is described by the discretized population balances, which simulate the changes of the molecular weight distribution during the extraction. The model governing equations with the initial and boundary conditions are:

Bulk phase:

$$\frac{\partial C_{bi}}{\partial t} + u\frac{\partial C_{bi}}{\partial z} + \frac{3k_i\left(1-\varepsilon_b\right)\left(C_{bi}-C_{pi,R=R_p}\right)}{\varepsilon_b R_p} - D_i\frac{\partial^2 C_{bi}}{\partial z^2} = \sum_{j=1}^{NC}\beta(L_i,L_j)\Delta L_i g(L_j)C_{bj} - g(L_i)C_{bi} \quad (4.4.1)$$

Stagnant liquid phase:

$$\frac{\partial C_{pi}}{\partial t} - \varepsilon_p D_{pi}\frac{1}{R^2}\frac{\partial}{\partial R}\left(R^2\frac{\partial C_{pi}}{\partial R}\right) = k_{di}C_{pi}^s + \sum_{j=1}^{NC}\beta(L_i,L_j)\Delta L_i g(L_j)C_{pj} - g(L_i)C_{pi} \quad (4.4.2)$$

Solid wood particle phase:

$$\frac{\partial C_{pi}^s}{\partial t} = -k_{di}C_{pi}^s + \sum_{j=1}^{NC}\beta(L_i,L_j)\Delta L_i g(L_j)C_{pj}^s - g(L_i)C_{pi}^s \quad (4.4.3)$$

The reaction term or source term $S(t,z)_{reation}$ in Eq.(4.1) and (4.2) is replaced by the discretized population balance term $\sum_{j=1}^{NC}\beta(L_i,L_j)\Delta L_i g(L_j)C_{bj} - g(L_i)C_{bi}$, to describe the degradation of polymers. The term $k_{di}C_{pi}^s$ in Eq.(4.4.2) and (4.4.3) is for the dissolution of polymers from the solid wood particle phase to the stagnant liquid phase.

Initial and boundary conditions of Eq. (4.4.1)-(4.4.3) are:

$$t = 0, \quad C_{bi} = C_{bi}(0,z), \quad C_{pi} = C_{pi}(0,R,z), \quad C_{pi}^s = C_{pi}^s(C_{0i},R,z) \tag{4.4.4}$$

$$z = 0, \quad \frac{\partial C_{bi}}{\partial z} = \frac{u C_{bi}}{D_i}; \quad z = L, \quad \frac{\partial C_{bi}}{\partial z} = 0 \tag{4.4.5}$$

$$R = 0, \quad \frac{\partial C_{pi}}{\partial R} = 0; \quad R = R_p, \quad \frac{\partial C_{pi}}{\partial R} = \frac{k_i}{\varepsilon_p D_{pi}} \left(C_{bi} - C_{pi, \, R=Rp} \right) \tag{4.4.6}$$

The initial condition of Eq.(4.4.4) describes that at $t = 0$, the hemicellulose polymers exist only in the solid wood particle phase. The concentration of hemicellulose polymers is zero in bulk phase and stagnant liquid phase.

Discretized population balance notion (Alopaeus et al., 2006) is applied in the model of this study. This results in a high number of variables to be solved because the hemicellulose polymers in the model are divided into approximately 20 categories based on the polymer chain length, which indicates 20 ODEs need to be solved. The moment method is used to solve the model of this work. Similar as any high order methods, the moment method is capable to reach expected accuracy with less number of variables (approximately 10^2-10^3 variables with the moment method in this work), resulting in faster computational speed than those low order methods. This is especially beneficial in this work because the number of integrated ODEs can reach to the range of 10^3-10^4 if low order method is applied. In addition, the mass balance error is limited into a satisfactory scope in all cases of this study (<0.2%), as one advantage of the moment method.

In this study, the model parameters are estimated by three methods. Some of model parameters are directly from the experimental setup (Leppänen et al., 2011), such as the extraction chamber dimensions, water flow speed, wood meal particle size, extraction temperatures etc. Secondly some parameters are estimated based on the published literature, such as wood particle porosity (Robertsen, 1993), Effective Capillary Cross Sectional Area (Törnqvist et al., 2001), pore diffusion coefficient (Reid, 1987), external film mass transfer coefficient (Wilson, 1966), axial dispersion coefficient (Chung and Wen, 1968), degradation rate (Visuri et al., 2012; Mittal et al., 2009), initial hemicellulose molecular weight distribution (Willför et al., 2003; Zhang et al., 2013) etc. Because the dissolution rates of the hemicelluloses in this work are not available in open literature, hence unknown parameters are fitted against experimental data. Two different schemes to model the dissolution rates are tested in this study:

Scheme 1:

$$k_d = \frac{b_1 e^{-b_2/RT_{tr}}}{DP} \tag{4.4.7}$$

Scheme 2:

$$k_d = b_1 e^{-b_2/RT_{tr}}$$ (4.4.8)

Where b_1 and b_2 are the two unknown parameters to fitted. DP is the Degree of Polymerization.

T_{tr} is the transposed temperature calculated as (Visuri et al. 2012):

$$\frac{1}{T_{tr}} = \frac{1}{T} - \frac{1}{T_{ave}}$$ (4.4.9)

Where T_{ave} is the average temperature of the experiments, T is the measured temperature in the experiments. T_{tr} is used in order to reduce excessive parameter cross-correlation during the parameter optimization (Rose 1981).

In addition, the degradation rates estimated by the empirical formulations provide relatively inaccurate simulation results compared to the experiments. Also according to the parameter sensitivity study in Publication [4], the degradation rate exerts considerable influence on the simulation results. Therefore, the values of degradation rate are also fitted against the experimental measurement results as Eq. (4.4.10).

$$g = b_3 e^{-b_4/RT_{tr}}$$ (4.4.10)

Where "g" is the degradation rate for individual bond. All bonds in a polymer, connecting the monomeric units, degrade at an equal degradation rate due to the assumption of random scission. b_3 and b_4 are the two unknown parameters to fitted. More detailed discussions of the estimation of parameters can be found in Publication [4].

In this study, our major objective is to simulate the average molecular weights (AMWs) in the extracts and compare to the measured results. In Figure 4.4.1, the dissolution rates at different temperatures are fitted against the measured out flow mass in the extracts (Leppänen et al., 2011). All the other parameters are estimated based on the published literature data. It can be seen that the deviations between the simulated and measured results are large.
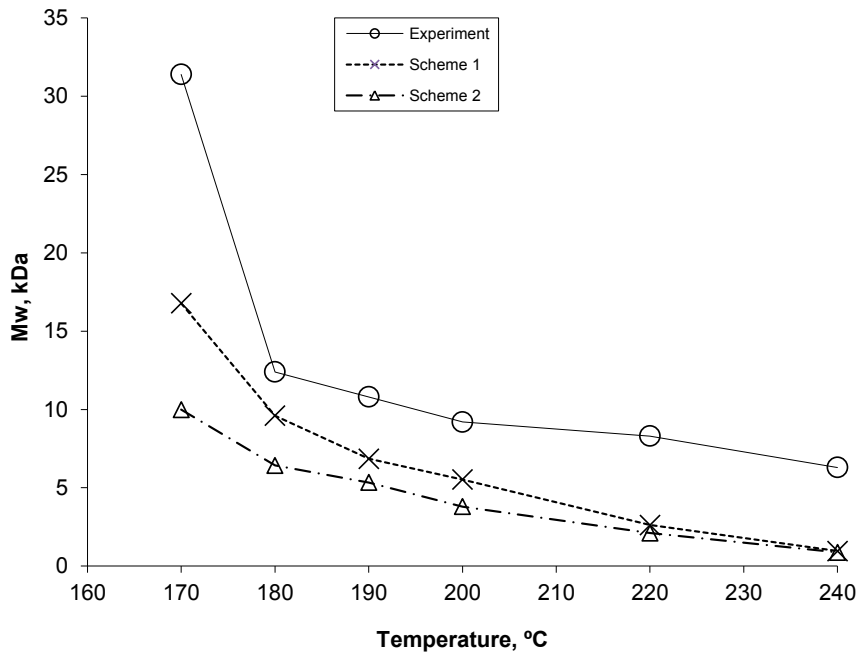
Figure. 4.4.1. Average molecular weights of hemicelluloses in water extracts, experimental data and simulation results. Only the dissolution rate model parameters were fitted.

In Figure 4.4.2, the dissolution rates and the degradation rates at different temperatures are fitted against the measured out flow mass and the measured AMWs in the extracts respectively. Good conformity is obtained between the simulated and measured results.
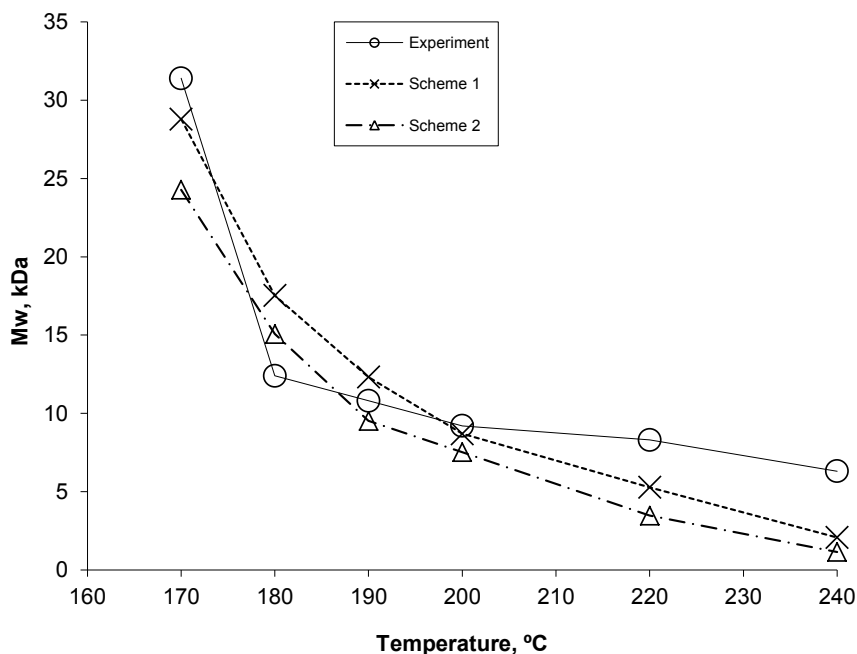
Figure. 4.4.2. Average molecular weights of hemicelluloses in water extracts, experimental data and simulation results. The dissolution rates and degradation rates were fitted.

The high performance size exclusion chromatography with multi-angle laser light scattering detection method (HP-SEC_MALLS) was used to determine the average molecular weights in the experiment (Leppänen et al., 2011), in which the small polymers might be overlooked during the measurement of AMWs of extracts, resulting in higher measured AMW values. This issue is only suspected by the experimentalists without confirmative evidences. To investigate it, we intentionally neglected those categories with smaller molecular masses (< 1kDa, <2kDa, <5kDa) in the outflow curves when calculating the simulated results of AMWs. From Figure 4.4.3, it can be seen that the simulated AMWs at low temperatures (170°C-200°C), are not affected much when ignoring the contributions of the smaller polymers. But the simulated AMWs increase clearly when the smaller polymers are excluded at higher temperatures (220°C, 240°C). The reason is that the faction of the smaller polymers in the extracts becomes considerable due to the larger degradation rates at higher temperatures. On the other hand, the conformity between the predicted and measured AMWs becomes quite satisfactory, e.g. in case when the polymers <5 kDa in the extracts are ignored for the simulation of AMWs, especially at higher temperatures. Based on the modeling results above, we have the reason to speculate that the measurement of AMWs of extracts might be inaccurate due to the unexpected ignorance on the molecular with smaller molecular masses.
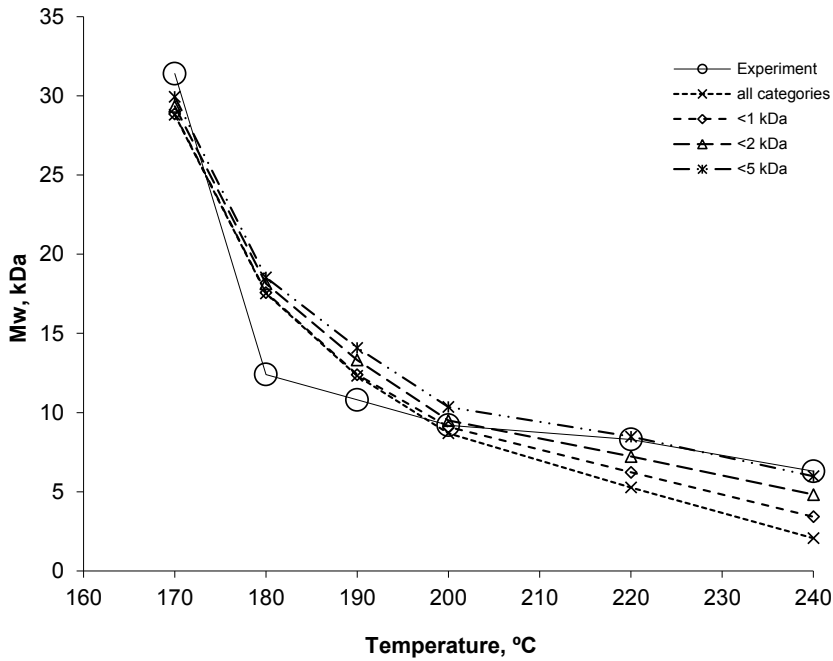
Figure. 4.4.3 Average molecular weights of hemicelluloses in water extracts, experimental and simulation results. Smaller polymers (<1kDa, <2kDa and <5kDa) are not considered in the simulation results. The dissolution rates and degradation rates were fitted.

Except the simulation of the AMWs in the extracts, the model developed in this study is able to predict the outflow mass from the extraction process. As shown in Figure 4.4.4, the simulated monosaccharides at different temperatures are compared with the measured results, which show satisfactory conformity.
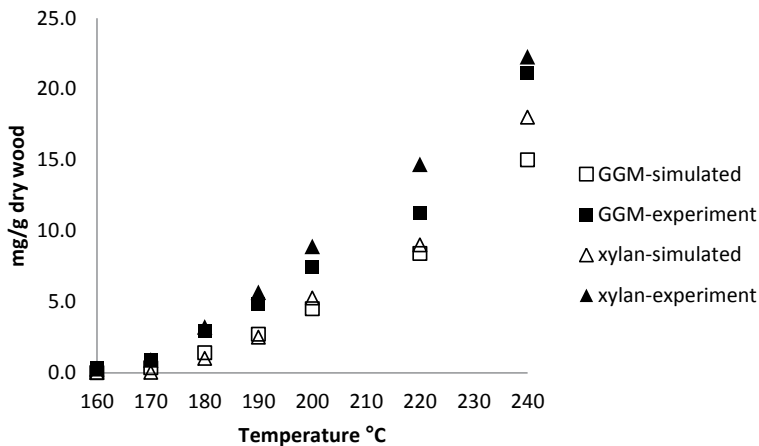
Figure 4.4.4. Simulated and measured amounts of monosaccharides of GGM and xylan

5. Conclusion

In this thesis, several applications of the moment method are presented and discussed. The application to solve the chromatographic general rate model suggests that the moment method is an efficient numerical tool which can be utilized to the chromatographic model, as well as to other similar models such as turbulent reactors, packed column etc.

One feature of the moment method is to minimize the errors of moments in the chromatogram. This suggests that the three characteristic values of the chromatogram, namely the retention time (related to 1st normalized moment), physical dispersion (related 2nd central moments) and skewness (related 3rd central moments) of the simulated effluent curve, are estimated with minimized errors. According to this, a number of parameters of the chromatographic model are optimized successfully with the utilization of these three characteristic values of the simulated effluent curves.

Similar with other high order methods, the moment method is capable to reach a desired accuracy with decreased number of variables and reduced computational load. Based on this nature, the moment method is used instead of the low order finite difference method in the case when the concentration profiles in the anisotropic biomass particle are modeled. The number of variables is decreased and the computational load is reduced significantly.

In the study of modeling the concentration profiles of hemicelluloses in the flow-through hot water extraction process, the number of coupled ODEs is unavoidably large. The advantage of the moment method appears again since the ODEs can be solved with limited computational time.

The goal of this PhD study is to utilize the moment method as a general solution method or numerical tool in practically applicable simulator or chemical engineering design tool. Gu (Gu et al., 1993) used the orthogonal collocation and finite element methods as the numerical tool in the solution of the chromatographic general rate model and commercialized the simulator in the 90s' of last century. The future work might focus on the development and applications of the moment method in the industrial simulators and other commercial design tools.

Symbols

[*A*]	[-]	linear operator between polynomial coefficients and distribution moments
A_{xy}	[m^2]	surface area of coordinate x and y
A_{xz}	[m^2]	surface area of coordinate x and z
A_{yz}	[m^2]	surface area of coordinate y and z
A_α	[m^2]	surface area of the particle
a	[-]	constant in Langmuir isotherm
Bi	[-]	Biot number, $\dfrac{kR_P}{\varepsilon_P D_P}$
b	[-]	constant in Langmuir isotherm
b_1	[-]	unknown parameter in dissolution rate models
b_2	[-]	unknown parameter in dissolution rate models
b_3	[-]	unknown parameter in degradation rate model
b_4	[-]	unknown parameter in degradation rate model
C	[mol L^{-3}]	concentration
C_b	[mol L^{-3}]	bulk phase concentration
C_f	[mol L^{-3}]	feed concentration profile, a time dependent variable
C_{ref}	[mol L^{-3}]	concentration used for nondimensionalization in chromatographic models
C_p	[mol L^{-3}]	concentration in stagnant fluid phase inside the particle macropores
C_p^s	[mol L^{-3}]	concentration in the solid phase of particle
C_0	[mol L^{-3}]	concentration used for nondimensionalization in isotherms
D	[m^2 s^{-1}]	axial dispersion coefficient
D	[m^2 s^{-1}]	diffusion coefficient in water
D_p	[m^2 s^{-1}]	pore diffusion coefficient
DP	[-]	degree of polymerization
E_x'	[-]	effective capillary cross sectional area at x coordinate
E_y'	[-]	effective capillary cross sectional area at y coordinate
E_z'	[-]	effective capillary cross sectional area at z coordinate
$g(L)$	[s^{-1}]	degradation rate of polymers with a size *L*
j	[molm^{-2} s^{-1}]	diffusion flux

K_r	[m^3 mol^{-1}s^{-1}]	reaction rate constant
k	[m s^{-1}]	film mass transfer coefficient
k	[-]	moment number
k	[J/K]	Boltzmann constant
k_{cm}	[m s^{-1}]	convection mass transfer coefficient
k_d	[s^{-1}]	dissolution rate
k_{xy}	[m s^{-1}]	lumped external film diffusion coefficient at the area of coordinate x and y
k_{xz}	[m s^{-1}]	lumped external film diffusion coefficient at the area of coordinate x and z
k_{yz}	[m s^{-1}]	lumped external film diffusion coefficient at the area of coordinate y and z
L	[m]	separation column length
L	[m]	particle characteristic dimension
M	[-]	moment of a chromatogram
m	[-]	moment of a distribution
M	[mol]	the number of moles
n	[-]	order of the profile polynomial
Pe	[-]	Péclet number, $\dfrac{uL}{D}$
R	[m]	spherical particle coordinate
R	[-]	residual
R_P	[m]	spherical particle radius
r	[-]	dimensionless spherical particle coordinate
r	[mol m^{-3}s^{-1}]	reaction rate
S	[kg m^{-3}s^{-1}]	dimensional source term
s	[-]	dimensionless source term
T	[K]	temperature
t	[s]	time
u	[m s^{-1}]	molar average velocity
V_α	[m^3]	volume of the particle
V_{bA}	[m^3]	molecular volume
w	[-]	weights, combined with basis functions to approximate the concentration profile
w	[-]	coefficients in the approximation function; weighting factor in the objective function

X	[m]	wood chip length of x coordinate
Y	[m]	wood chip length of y coordinate
Z	[m]	wood chip length of z coordinate
z	[m]	axial coordinate

Greek symbols

θ	[-]	dimensionless time
ϕ	[-]	angle of position in spherical coordinate
ω	[-]	colatitude in spherical coordinate
η	[-]	dimensionless constant, $\dfrac{\varepsilon_P D_P L}{R_P^2 u}$
$\beta(L_i, L_j)$	[-]	daughter size distribution for the breakage of larger polymers L_j forming smaller L_i sized polymers
$\beta(L_i, L_j)\Delta L_i$	[-]	contribution of breakage from category *j* into category *i*
ΔL	[-]	size of a category
ε_{xy}	[-]	porosity at the area of coordinate x and y
ε_{xz}	[-]	porosity at the area of coordinate x and z
ε_{yz}	[-]	porosity at the area of coordinate y and z
ε_b	[-]	bed porosity
ε_p	[-]	particle porosity
ψ_b	[-]	dimensionless bulk phase concentration
ψ_p	[-]	dimensionless concentration in particle macropore phase
ψ_p^s	[-]	dimensionless concentration in particle solid phase
ξ	[-]	dimensionless constant, $\dfrac{3 Bi\,\eta(1-\varepsilon_b)}{\varepsilon_b}$
ζ	[-]	dimensionless axial coordinate
μ	[-]	mean of the effluent curve

μ	[cP]	dynamic viscosity
σ	[-]	standard deviation of the effluent curve
γ	[-]	skewness of the effluent curve
τ	[-]	particle tortuosity
Ω	[-]	geometrical shape parameter
j	[mol m^{-2}s^{-1}]	flux
Φ	[-]	Associative factor of solvant

Subscripts and superscripts

0	initial value, boundary value
b	bulk phase
i	index
j	index or j^{th} moment
k	index
NC	total number of categories
p	pore phase in particle
ref	reference value
s	stationary phase in particle

References

Alopaeus, V., Laakkonen, M., Aittamaa, J. (2006): Solution of population balances with breakage and agglomeration by high-order moment-conserving method of classes. *Chemical Engineering Science.* 61 (20), 6732-6752.

Alopaeus, V., Laavi, H., Aittamaa, J. (2008). A dynamic model for plug flow reactor state profiles. *Computers and Chemical Engineering. 32*, 1494-1506.

Atkinson, Kendall A. (1989). *An Introduction to Numerical Analysis* (2nd ed.). New York: John Wiley & Sons.

Bird, R.B., Stewart, S.E., Lightfoot, E.N. (1960). *Transport Phenomena*, John Wiley & Sons, New York, NY

Burghardt, A., Kubaczka, A. (1996). Generalization of the effectiveness factor for any shape of a catalyst pellet. *Chemical Engineering and Processing: Process Intensification.* 35*, 65-74.*

Chen, T., Zhang G.L., (2001). *Hua Gong Chuan Di Guo Cheng Ji Chu*. Beijing: Hua Gong Chu Ban She.

Chung, S.F., Wen, C.Y. (1968). Longitudinal Dispersion of Liquid Flowing Through Fixed and Fluidized Beds. *AIChE J.*, 14, 857-866

Danckwerts, P.V. (1951). Significance of liquid-film coefficients in gas absorption. *Industrial and Engineering Chemistry*, 43 1460–1467

Date, Anil W. (2005). *Introduction to Computational Fluid Dynamics*, Cambridge University Press

Einstein, A. (1905). *Ann. der Physik*, 17, 549

Ferziger, J.H., Peric, M., 2002. Computational Methods for Fluid Dynamics. 3rd ed. Berlin: Springer-Verlag.

Finlayson, B. A., (1972). *The Method of Weighted Residuals and Variational Principles.* New York: Academic Press.

Finlayson, B. A., (1980). *Nonliear Analysis in Chemical Engineering.* New York: McGraw-Hill.

Fletcher, C. A. J., (1991*). Computational Techniques for Fluid Dynamics. Volume 1. Fundamental and General Techniques. 2nd ed.* Berlin: Springer-Verlag.

Golshan-Shirazi, S., Guiochon, G. (1989). Analytical solution of the ideal model of elution chromatography in the case of a binary mixture with competitive Langmuir isotherms. II. Solution using the h-transform. *Journal of Chromatography, 484,* 125-151

Golshan-Shirazi, S., Guiochon, G. (1989). Analytical solution for the ideal model of chromatography in the case of a pulse of a binary mixture with competitive langmuir isotherm. *Journal of Physical Chemistry, 93 (10),* 4143-4157

Grénman, H., Wärnå, J., Mikkola, J.-P., Sifontes, V., Fardim, P., Murzin, D.Y., Salmi, T. (**2010***).* Modeling the influence of wood anisotropy and internal diffusion on delignification kinetics*. Industrial and Engineering Chemistry Research. 49*, 9703-9711.

Gu, T., Tsai, G-J., Tsao, G.T. (1990). New approach to a general nonlinear multicomponent chromatography model. *AIChE Journal, 36(5)*, 784

Gu, T., Tsai, G.-J., Tsao, G.T. (1993). Modeling of nonlinear multicomponent chromatography. *Advances in Biochemical Engineering Biotechnology, 49*

Harten, A., Engquist, B., Osher, S., Chakravarthy, S. (1987). Uniformly high order essentially non-oscillatory schemes, *III, Journal of Computational Physics*, 71, 231-303

Higbie., R. (1935). The rate of absorption of a pure gas into a still liquid during short periods of exposure. *Transactions of the American Institute of Chemical Engineers*, 31, 365–389

Hines, A., Maddox, R., (1985) Mass transfer: Fundamentals and Applications, Prentice Hall, NJ.

Hirsch, C. (1990). Numerical Computation of Internal and External Flows. Volume 2: Computational Methods for Inviscid and Viscous Flows, Wiley

Jiang, G., Shu, C.-W. (1996). Efficient implementation of weighted ENO schemes, Journal of Computational Physics, 126:202-228.

Jutila, E. A. A. (1980). A Survey of Kraft Cooking Control Models. *Instrumentation and Automation in the Paper, Rubber, Plastics and Polymerization Industries, Proceedings of the 4th IFAC Conference.* Oxford.

Leppänen, K., Spetz, P., Pranovich, A., Hartonen, K., Kitunen, V., Ilvesniemi, H. (2011). Pressurized hot water extraction of Norway spruce hemicelluloses using a flow-through system. *Wood Science and Technology. 45*, 223-236.

Lewis, WK., Whitman, WG. (1924). Principles of gas absorption, *Industrial & Engineering Chemistry,* ACS Publications

Liong, K.K., Wells, P.A., Foster, N.R. (1991). *J. Supercrit. Fluids* 4, 91.

Liu, X.-D. , Osher, S., Chan, T. (1994). Weighted essentially non-oscillatory schemes, Journal of Computational Physics, 115:200-212.

Mackie, J.S., Meares, P. (1955). The Sorption of Electrolytes by a Cation-Exchange Resin Membrane. *Proc. R. Soc. A*., 232, 485

Mittal, A., Chatterjee, S.G., Scott, G.M., Amidon, T.E. (2009). Modeling xylan solubilization during autohydrolysis of sugar maple and aspen wood chips: Reaction kinetics and mass transfer. *Chemical Engineering Science*. 64, 3031-3041.

Miyabe, K. (2008). Evaluation of chromatographic performance of various packing materials having different structural characteristics as stationary phase for fast high performance liquid chromatography by new moment equations. *J. Chromatogr. A.*, 1183, 49-64

Miyabe, K. (2009). Moment Analysis of Chromatographic Behavior in Reversed-Phase Liquid Chromatography. *J.Sep.Sci.*, 32, 757

Reddy, J.N. (2005). *An Introduction to the Finite Element Method* (Third ed.). McGraw-Hill.

Reid, R. C., Prausnitz, J. M., Poling, B. E. (1987). *The Properties of Gases and Liquids.* McGraw-Hill, New York, USA.

Rice, R.G., Do, D.D., (1995). *Applied Mathematics and Modeling for Chemical Engineers.* New York: John Wiley & Sons

Robertsen, L. (1993). *Diffusion in wood: Part 4. Diffusion in radial and longitudinal direction* [dissertation]. Department of pulping technology, Abo Akademi.

Roininen, J., Alopaeus, V. (2011). The moment method for one-dimensional dynamic reactor models with axial dispersion. *Computers and Chemical Engineering, 35(3),* 423-433.

Roininen, J. (2010). *Process equipment modeling using the moment method* [dissertation]. Department of Biotechnology and Chemical Technology, Aalto University.

Rose, L. M. (1981). *In Chemcial Reactor Design in Practice*; Elsevier: Amsterdam.

Saari, P., Heikkilä, H., Hurme, M. (2010). Adsorption equilibria of arabinose, fructose, galactose, glucose, mannose, rhamnose, sucrose, and xylose on ion-exchange resins. *J. Chem. Eng. Data*, *55*, 3462

Samarskii, A.A. (2011). *The Theory of Difference Schemes*. CRC Press

Schiesser, W. E., Griffiths, G. W. (2009). *A Compendium of Partial Differential Equation Models: Method of Lines Analysis with Matlab*. Cambridge University Press.

Siitonen, J., Sainio, T. (2011). Explicit equations for the height and position of the first component shock for binary mixtures with competitive Langmuir isotherms under ideal conditions. *Journal of Chromatography A, 1218 (37),* 6379-6387

Sweby, P.K. (1984). "High resolution schemes using flux-limiters for hyperbolic conservation laws", SIAM J. Num. Anal. 21 (5): 995–1011

Taylor, R., Krishna, R., (1993*). Multicomponent Mass Transfer.* New York: John wiley & Sons.

Thibodeaux, L., Mackay, D. (2011) *Handbook of Chemical Mass Transport in the Environment*. CRC Press

Turku, I., Sainio, T. (2009). Modeling of adsorptive removal of benzalkonium chloride from water with a polymeric adsorbent. *Separation and Purification Technology, 69,* 185-194

Törnqvist, M., T. Hurme, J.B. Rosenholm. (2001). The concentration dependence of the diffusion coefficient in Pine, Birch and Spruce. *Pap. Puu.* 83(3), 204-209.

Villadsen, J., Michelsen, M. (1978). *Solution of differential equation models by polynomial approximation.* Prentice-Hall, INC.

Visuri, J.A., Song, T., Kuitunen, S., Alopaeus, V. (2012). Model for degradation of galactoglucomannan in hot water extraction conditions. *Industrial and Engineering Chemistry Research.* 51 (31), 10338-10344.

Wang, F., (2004). *Ji Suan Liu Ti Li Xue Fen Xi-CFD software theories and applications*. Tsinghua Press: Beijing.

Wesseling, Pieter (2001). *Principles of Computational Fluid Dynamics*, Springer-Verlag.

Wilke and Chang, (1955). AIChE J. 1, 264

Willför, S., Sjöholm, R., Laine, C., Roslund, M., Hemming, J., Holmbom, B. (2003). Characterisation of water-soluble galactoglucomannans from Norway spruce wood and thermomechanical pulp. *Carbohydrate Polymers*. 52 (2), 175-187.

Wilson, E.J., Geankoplis, C.J. (1966). Liquid Mass Transfer at Very Low Reynolds Numbers in Packed Beds. *Ind. Eng. Chem. Fundam.*, 5, 9-14

Zhang, Y., Li, J., Lindström, M.E., Stepan, A., Gatenholm, P.(2013). Spruce glucomannan: Preparation, structural characteristics and basic film forming ability. *Nordic Pulp and Paper Research Journal.* 28, 323.

BUSINESS +
ECONOMY

ART +
DESIGN +
ARCHITECTURE

SCIENCE +
TECHNOLOGY

CROSSOVER

**DOCTORAL
DISSERTATIONS**